J Bioenerg Biomembr (2009) 41:195–214
DOI 10.1007/s10863-009-9214-x

# Mitochondrial dynamics in heart cells: Very low amplitude high frequency fluctuations in adult cardiomyocytes and flow motion in non beating Hl-1 cells

**Nathalie Beraud · Sophie Pelloux · Yves Usson · Andrey V. Kuznetsov · Xavier Ronot · Yves Tourneur · Valdur Saks**

Received: 16 February 2009 / Accepted: 18 March 2009 / Published online: 28 April 2009


**Abstract** The arrangement and movement of mitochondria were quantitatively studied in adult rat cardiomyocytes and in cultured continuously dividing non beating (NB) HL-1 cells with differentiated cardiac phenotype. Mitochondria were stained with MitoTracker® Green and studied by fluorescent confocal microscopy. High speed scanning (one image every 400 ms) revealed very rapid fluctuation of positions of fluorescence centers of mitochondria in adult cardiomyocytes. These fluctuations followed the pattern of random walk movement within the limits of the internal space of mitochondria, probably due to transitions between condensed and orthodox configurational states of matrix and inner membrane. Mitochondrial fusion or fission was seen only in NB HL-1 cells but not in adult cardiomyocytes. In NB HL-1 cells, mitochondria were arranged as a dense tubular network, in permanent fusion, fission and high velocity displacements of ~90 nm/s. The differences observed in mitochondrial dynamics are related to specific structural organization and mitochondria-cytoskeleton interactions in these cells.

**Keywords** Mitochondria · Movement · Cardiomyocytes · NB HL-1 cells · Image analysis · Fluctuations · Fusion · Fission

## Introduction

Mitochondrial functioning is associated, in many cells, with dynamic changes in morphology of these organelles, and also with their movement. The earliest indications of dynamic

**Electronic supplementary material** The online version of this article (doi:10.1007/s10863-009-9214-x) contains supplementary material, which is available to authorized users.

N. Beraud · V. Saks
INSERM U884, Laboratory of Fundamental and Applied Bioenergetics, Joseph Fourier University, Grenoble, France

S. Pelloux · Y. Tourneur
INSERM U886, Centre Commun de Quantimétrie, Université Lyon 1, Université de Lyon, Lyon, France

Y. Usson
CNRS UMR5525, TIMC-IMAG, Joseph Fourier University, Grenoble, France

A. V. Kuznetsov
D.Swarovski Research Laboratory, Department of Transplant Surgery, Innsbruck Medical University, Innsbruck, Austria

X. Ronot
Laboratoire de Dynamique Cellulaire, UMR 5525, UJF-CNRS-INPG-EPHE-ENVL, Grenoble, France

V. Saks
Laboratory of Bioenergetics, National Institute of Chemical Physics and Biophysics, Tallinn, Estonia

N. Beraud
Laboratory of Systems Biology, Institute of Cybernetics, Tallinn Technical University, Tallinn, Estonia

V. Saks (✉)
Laboratory of Bioenergetics, Joseph Fourier University, 2280, Rue de la Piscine, BP53X-38041 Grenoble Cedex 9, France
e-mail: Valdur.Saks@ujf-grenoble.fr

changes in mitochondrial morphology were obtained in the classical electron microscopic studies by Hackenbrock et al. (Hackenbrock 1966, 1968a, b) who showed morphological changes of isolated mitochondria from condensed (contracted matrix and expanded intracristal compartments) to orthodox (matrix expanded) configurations during transition from high (State 3) to low (State 4) respiration rates. Three-dimensional images of these changes were obtained by electron tomography in Mannella's laboratory (Mannella et al. 1997; Mannella 2001, 2006). Changes in the configuration of mitochondria related to the functioning of adenine nucleotide translocator (ANT) can also be easily recorded spectrophotometrically as changes in the turbidity (optical density) of mitochondrial suspensions *in vitro* (Weber and Blair 1970; Stoner and Sirak 1973; Scherer and Klingenberg 1974). *In situ* studies of mitochondria initiated by pioneering works by Bereiter-Hahn (1990) with application of optical methods led to the discovery of fusion and fission of mitochondria associated with the formation of a mitochondrial reticulum in some types of cells (Bereiter-Hahn 1990; Bereiter-Hahn and Voth 1994). In living cells mitochondrial behavior may be very different from that of isolated mitochondria *in vitro*, mostly because of their interaction with other cellular structures like the cytoskeleton (Milner et al. 2000), the endo(sarco)plasmic reticulum (Hajnóczky et al. 2000; Pacher et al. 2000; Rizzuto et al. 1998; Csordás et al. 2006), and because of the specific structure, organization and composition of intracellular medium. In the cells *in vivo* mitochondria are involved in structurally and functionally organized networks of integrated energy metabolism (Aon et al. 2007; Dzeja et al. 2007; Saks et al. 2007; Wallimann et al. 2007). Because of all these interactions, mitochondria in the cells *in vivo* acquire new, system-level properties, which are not predictable on the basis of *in vitro* isolated studies (Saks et al. 2007; Weiss et al. 2006). In many types of living cells, rapid fission, fusion and translocation events lead to continuous remodeling of the mitochondrial network (Yaffe 1999; Dimmer and Scorrano 2006; Kuznetsov 2007; Chan 2006; Benard and Rossignol 2008; Karbowski and Youle 2003). Mitochondrial organization into networks has spurred investigations into how they communicate with each other (Aon et al. 2007; Saks et al. 2007; Romashko et al. 1998; Skulachev 1990; Skulachev et al. 2004; McBride et al. 2006). Morphologically, distinct mitochondria can be arranged by the cytoskeleton into a regular lattice-like network, as in heart and many other cells (Aon et al. 2004; Vendelin et al. 2005; Collins et al. 2002) or form by fusion irregular, filamentous structures, as in neurons or cancer cells (Dimmer and Scorrano 2006; Karbowski and Youle 2003; Dedov and Roufogalis 1999). In muscle cells the mitochondrial intracellular arrangement has been found to be very regular and to follow the crystal-like pattern of modular organization (Vendelin et al. 2005; Birkedal et al. 2006). Modular organization means that mitochondria form very regularly arranged units (modules) with surrounding cellular structures which were called intracellular energetic units, ICEUs (Saks et al. 2001; Seppet et al. 2001). However, it is not clear whether mitochondria are completely immobilized within ICEUs, or whether they can undergo some kind of dynamic changes similar to those observed by Hackenbrock et al. (Hackenbrock 1966, 1968a, b) in isolated mitochondria *in vitro*. Equally important is to know whether mitochondrial fusion and fission may occur in muscle cells. Therefore, the aim of this work was to characterize quantitatively structural organization, mitochondrial dynamics and movements in two different types of heart cells: adult cardiomyocytes and non beating HL-1 (NB HL-1) cells by using confocal microscopy and newly developed methods of image analysis for determining the character and the rates of the movements of mitochondria inside the cells. NB HL-1 cells were chosen as a reference system because they exhibit characteristics of differentiated cardiac cells but are structurally and metabolically very different from adult cardiomyocytes (Anmann et al. 2006; Eimre et al. 2008; Claycomb et al. 1998; Pelloux et al. 2006). The results clearly show that under normal conditions fusion and fission of mitochondria are not seen in adult cardiomyocytes, in which, however, mitochondria undergo very rapid, low amplitude fluctuations, probably as a result of fast transitions between condensed and orthodox configurational states of matrix and inner membrane due to functioning of transmembrane metabolite carriers. However, mitochondrial fusion and fission are clearly seen in the HL-1 cells where mitochondria often form dynamic filamentous networks. The observed differences are related to specific structural organization of the cells, probably due to differences in mitochondria-cytoskeletal organization.

## Materials and methods

### Cardiomyocytes isolation

Adults cardiomyocytes were isolated as described previously (Anmann et al. 2006). Wistar male rats (300 g) were anaesthetized by pentobarbital with the addition of 500 U of heparin. The heart was quickly excised preserving a part of aorta and placed into filtered (0.45 μm) aerated isolation medium (IM) of the following composition: 117 mM NaCl, 5.7 mM KCl, 4.4 mM $NaHCO_3$, 1.5 mM $KH_2PO_4$, 1.7 mM $MgCl_2$, 11.7 mM glucose, 11 mM Cr, 20 mM taurine, 10 mM phosphocreatine, 21.1 mM HEPES, 2 mM pyruvate, pH 7.1 at 25°C. The heart was cannulated and washed with the aerated IM during 5 min with a flow rate of 15–20 ml/min. The heart was digested by perfusion with isolation medium, recirculating in a closed system with a flow rate of 5 ml/min, containing 1 mg/ml collagenase type II (Roche) and 20–25 μM of free calcium. The end of the digestion was determined

following the decreasing of perfusion pressure measured by a manometer. After the digestion, the heart was washed with the IM during 2–3 min and placed into IM containing 20 μM free calcium, 4.7 μg/ml leupeptin, 0.56 mg/ml trypsin inhibitor and 2 mg/ml BSA. It was disrupted mechanically by forceps to release the cardiomyocytes. The cell suspension was filtered and transferred into a tube for sedimentation during 3–5 min at room temperature. Sedimentation with 20 μM free calcium was repeated twice. Cardiomyocytes were gradually transferred from isolation medium (with 20 μM free calcium and 2 mg/ml BSA) into Mitomed (110 mM sucrose, 60 mM K-lactobionate, 0.5 mM EGTA, 3 mM $MgCl_2$, 0.5 mM dithiothreitol, 20 mM taurine, 3 mM $KH_2PO_4$, 20 mM K-HEPES, pH 7.1 at 25°C) in three steps. Cardiomyocytes were washed 3 times with the Mitomed solution. Each time, the supernatant was removed after cell sedimentation. Isolated cells were stored at 4°C in the last solution until confocal microscopy experiments. Isolated cardiomyocytes contained 60–90% of rod-like cells when observed under the microscope.

In all confocal microscopic studies of mitochondrial dynamics, the respiratory substrates (glutamate 5 mM and malate 2 mM) and BSA (2 mg/mL) were added in Mitomed medium. Permeabilization of cardiomyocytes was carried out by incubation of cardiomyocytes with saponin (25 μg/ml) at room temperature. For selective proteolysis of cytoskeletal proteins, trypsin was added to a final concentration of 0.2 mg/ml.

## NB HL-1 cells culture

Non beating HL-1 cells (NB HL-1) were cultured as described previously (Claycomb et al. 1998; Pelloux et al. 2006) at 37°C under 5% CO2 in fibronectin-gelatin coated slides in supplemented Claycomb medium (JRH Biosciences) with 10% fetal bovine serum (JRH Biosciences), 100 U/ml penicillin, 100 μg/ml streptomycin (Invitrogen), 2 mM L-glutamine (Invitrogen), 10 μM norepinephrine and 0.3 mM ascorbic acid (Sigma).

## Confocal imaging of mitochondria dynamics in living cells

To monitor the mitochondrial functional state at the level of the single mitochondrion, images were acquired and analyzed by fluorescent confocal microscopy.

For mitochondrial imaging (localization) studies, cells were loaded with 0.2 μM mitochondrial specific probe MitoTracker® Green (Molecular Probes, Eugene, OR) which becomes fluorescent in lipid environments after binding to mitochondrial proteins by reacting with free thiol groups of cysteine residues, and therefore is insensitive to membrane potential (Presley et al. 2003) (see also the "Results" section). Before analysis, cardiomyocytes were incubated with probe at least 2 hours at 4°C in a Heraeus Flexiperm chambers (Hanau, Germany) and NB HL-1 cells in the chambered coverglass (Nalge Nunc, Rochester, NY) under standard incubator conditions (37°C, 5% $CO_2$).

To analyze mitochondrial inner membrane potential, cells were incubated for 30 min with 50 nM tetramethylrhodamine methyl ester (TMRM, Sigma), a fluorescent dye that accumulates in mitochondria on the basis of their membrane potential when added directly to the cell culture medium. In control experiments dissipation of membrane potential was observed after addition of 5 μM antimycin A (Sigma) and 4 μM FCCP (carbonyl cyanide-*p*-trifluoromethoxyphenyl-hydrazone, Sigma) (data not shown).

To localize the nucleus in NB HL-1 cells, the cell permeable nucleic acid probe Hoechst 33342 (DNA bound) was used.

The transmission and fluorescent images were acquired with an inverted confocal microscope (Leica DM IRE2) with a 63-x water immersion lens. The MitoTracker® Green fluorescence was excited with the 488 nm line of an argon laser, using 510 to 550 nm range for detection of emission. TMRM fluorescence was measured using 543 nm for excitation (Helium-Neon laser) and greater than 580 nm for emission. Hoechst 33342 was excited with UV light at 350 nm and has a maximal emission at 461 nm.

Table 1 shows the acquisition parameters of time series images.

## Image analysis

### *Analysis of mitochondrial fluctuations in adult cardiomyocytes using the gradient clustering algorithm method*

The contents of time series recordings were rotated in order to align the great axis of the myocardial cell with the horizontal axis of the image. This rotation operation was applied in order to give to all image stacks a common reference system such that the motions can be compared from one series to another.

*Image processing approach: Gradient clustering algorithm*
The number of mitochondria and the position of their fluorescence centers, or virtual mass centers, were automatically calculated by a gradient clustering algorithm (Fukunaga and Hostetler 1975). Basically this algorithm relies on a physical analogy: here a fluorescent pixel is considered as a physical object characterized by a couple of

**Table 1** Parameters of time series image acquisition in rapid scan confocal microscopy for cardiomyocytes and NB HL-1 cells

| Preparation | Image size, pixels | Pixel dwell time | Δt between images |
|---|---|---|---|
| Cardiomyocytes | 256×256 | 3.09 μs/pixel | 401 ms |
| NB HL-1 cells | 512×512 | 3.18 μs/pixel | 834 ms |

coordinates $x$ and $y$ (*i.e.* the initial position on the image grid) and a weight (or virtual mass) equal to the fluorescence intensity at this point. The concentration of virtual masses (fluorescence intensities) in particular regions of the images (*i.e.* mitochondria) creates so called "gravitational wells" attracting the neighbouring points. Actually, the algorithm calculates local intensity gradients in order to aggregate in an iterative manner the points belonging to the same mitochondrion. After a number of iterations these points will occupy a single position corresponding to the mass center of the mitochondrion, which acts as a gravitational attractor.

Explained in a pragmatic way, at the beginning, all of the pixels of the images with a fluorescence intensity greater than a fixed threshold are converted into points defined by their coordinates (x,y) and an associated mass (m) which corresponds to the pixel intensity. On each image, the mass center within a fixed neighborhood is calculated. After one iteration step each point is translated toward the nearest mass center, traveling a fraction of the distance between its initial position and the mass center. The sum of all the resulting point motions is calculated and used as a criterion to monitor the clustering process. The process is iterated until this sum falls under a preset value for which it is considered that the clustering process is achieved. To complete the algorithm, a merging procedure is applied where all the points with the same coordinates are merged into a unique point, which is considered as the mass center of a single mitochondrion. Using this clustering technique and under the hypothesis of an invariant Point Spread Function, it was possible to obtain the location of the fluorescence centers with a better accuracy than the actual optical resolution. The positions of these fluorescence centers directly depend on the configuration of the inner mitochondrial membrane to which the fluorescent dye used is fixed.

Complete description of all these calculations is given in the "Appendix" and additional explanations are available from Yves Usson at the address *yves.usson@imag.fr*.

*Quantification of mitochondrial fluctuations* The trajectories of the fluorescence centers were plotted as a function of time and the average scatters parallel to the long axis of the myocardial cells and to the short axis were calculated for each mitochondrion.

In order to express the motion behaviour of mitochondrial fluorescence centers in terms of a random-walk movement process, similar to Brownian movement of particles [50–55], the average squared distances ($d^2$) as a function of lag time ($t$) were plotted using two models: second order polynomial or linear. The fitted mean second order polynomial curve ($d^2=at^2+bt+c$) models the motion behaviour as a combination of random walk and a translational process. In such a model the $a$ constant may be assimilated to the apparent velocity component, and the $b$ constant relates with the apparent mobility constant $D$. The apparent mobility constant $D$ is analogous to the apparent diffusion constant and was determined from the slope $b$ of the fitted mean square linear curve ($d^2=bt+c$). In this expression, the parameter $c$ is related to the initial coordinates of the mitochondrial centers studied. For $c=0$ this expression can be reduced to the expression $d^2=bt$, which may be taken to be equivalent to a general expression for random-walk mechanism based on the Einstein-Smoluchowski's equation (Einstein 1905; von Smoluchowski 1906) for Brownian movement in two dimensions, $d^2=4Dt$, which gives the relationship between diffusion coefficient, $D$, distance of displacement, d, and time, t, of this displacement t (Philbert 2006; Islam 2004; Agutter et al. 1995; 2000). Thus, the apparent mobility constant $D$ calculated from the slope $b$ of the fitted mean square linear curve ($d^2=bt+c$) can be used as a quantitative measure of fluctuations of the fluorescence centers of mitochondria.

*Analysis of mitochondrial motions in NB HL-1 cells using Image Correlation Spectroscopy (ICS) method*

The dynamic behavior of the mitochondrial network was characterized using Image Correlation Spectroscopy (Wiseman and Petersen 1999; Wiseman et al. 2005; Margieantu et al. 2000).

*Pre-processing of time series images* Two successive pre-processings were applied to the stack of time series images in order to, first, compensate for photobleaching, and, second, to enhance the spatial resolution of the mitochondrial network. The reason of why it was important to correct for the effect of photobleaching was that the decrease in fluorescence intensity throughout the series would create a dominating flow component as an artefact in the auto-correlation curves.

In order to compensate for photobleaching, the average fluorescence intensity was calculated for each image in the time series. Next, a curve of the average intensity versus time was built and filtered using a wavelet filtering approach in order to extract the slow component of the curve corresponding to the photobleaching. Using this slow component as reference, a gain versus time compensation was applied to each image in order to correct the effect of photobleaching.

Enhancement of the mitochondrial network was performed using a mathematical morphology filtering. This was obtained by subtracting the result of a morphological closure (combination of grey level shrinking and grey level dilation of the image) from the image. The radius of the structuring kernel for the morphological closure was set to a value corresponding to the average width of mitochondrial filaments.

*Calculation of autocorrelation curves* The autocorrelation curves were calculated within so-called Regions of Interest (ROI), which are user defined subsets of the image. The

shape of such a ROI may be a regular geometric figure (rectangular, ellipse) or defined by a free hand drawing.

The temporal autocorrelation is a way of revealing the self-similarities of a signal. It consists of calculating the intersection of a curve with a time-shifted copy of this curve, the amount of shift being the lag time $\tau$.

The autocorrelation curve for a ROI containing $m$ pixels $p$ was caluculated as follows:

$$G(\tau) = \frac{1}{m \cdot t_{\max}} \sum_{t=1}^{t_{\max}} \frac{\sum_{j=1}^{m} \left[ \left( p_{j,t} - \mu_t \right) \cdot \left( p_{j,t+\tau} - \mu_{t+\tau} \right) \right]}{\mu_t \cdot \mu_{t+\tau}}$$

Where $G(\tau)$ is the autocorrelation function, $m$ is the number of pixels in the ROI, $p_{j,t}$ the fluorescence intensity measured in the $j^{th}$ pixel in image $t$, $j$ is the index of a pixel within the ROI, $n$ is the number of image in the time series, $t$ is the index of an image in the time series, $\tau$ is autocorrelation lag time, $t_{max}$ is equal to $n-\tau$; then $\mu_\tau$ and $\mu_{t+\tau}$ are the average intensities in the ROI in images $t$ and $t+\tau$, respectively.

*Interpretation of the autocorrelation curves* The autocorrelation curves were interpreted using the non-linear fitting tool of the *xmgrace* software (public domain, http://plasma-gate.weizmann.ac.il/Grace/), which is based on a classical Levenberg-Marquardt algorithm. The fitting procedure was supervised and several models were put to test in various combinations; the final combination was adopted being the one resulting in the smallest values of $\chi^2$ (chi-square) and residual error.

The usual models used for curve fitting were:

$$\textit{free diffusion}: \; G(\tau) = \left[ 1 + \frac{\tau}{\tau_D} \right]^{-1}, \; \textit{anomalous diffusion}: \; G(\tau) = \left[ 1 + \left( \frac{\tau}{\tau_A} \right)^{\alpha} \right]^{-1}, \; \textit{and flow}: \; G(\tau) = e^{-\frac{r^2}{\tau_V^2}}$$

where $\tau_D$ is the characteristic diffusion time from which the mobility (diffusion) constant can be derived, $\tau_v$ is the characteristic flow time from which the flow velocity can be derived, $\tau_A$ is the characteristic anomalous diffusion time from which the anomalous diffusion constant can be derived, and $\alpha$ the anomalousness parameter which is 1 for normal diffusion.

The values of the apparent general mobility constant equivalent to diffusion constant, and the apparent flow velocity were obtained using the following formulas of random walk type movement of particles (Philbert 2006; Islam 2004; Agutter et al. 1995; 2000): Apparent diffusion constant: $D = \frac{r^2}{4\tau_D}$; Apparent flow velocity: $v = \frac{r}{\tau_V}$.

The parameter $r$ corresponds to the size of measurement in pixels. The apparent flow velocity $v$ is the generalized resultant velocity of displacement between initial and final points (see Scheme 1).

*Analysis of mitochondrial motions in NB HL-1 cells using the distance map method*

Confocal images of the mitochondrial network stained with Mitotracker Green FM as described above were analyzed using Image J software (NIH, Bethesda, MD) as described before (Pelloux et al. 2005). Raw images were improved by filtering out the objects smaller than 3 pixels by Fast Fourier Transformation. Copies of these smoothed images were filtered with a 7 pixel wide Gaussian filter. Binary images were made from every grey image by applying a threshold to eliminate the fluorescence intensity factor. In order to focus only on mitochondria positions, binary images were then thinned until forming binary skeletons, which represent central positions of mitochondria. In the next step, distance maps *Di* were computed, which are images of the distance to the nearest point from the skeleton. In the last step, the binary skeletons at time *i+1*, *Si+1* was laid over the distance images *Di*. In the absence of movement, the pixel value on the distance map below skeleton is zero. If a movement occurred between the two images, the pixel value below the skeleton indicates the distance ran between times *i* and *i+1*. The average value of the pixel to pixel multiplication of *Si+1* and Di quantifies the average displacement between two successive images. This method gives the real instantaneous velocity of movement of mitochondrial centers (see Scheme 1). Thus, the application of two complementary methods described in the sections 4.2. and 4.3 gives complete information about dynamic changes of mitochondrial positions in the NB HL-1 cells (see Scheme 1).

## Results

### Mitochondrial organization and dynamics in adult cardiomyocytes

*Organized mitochondria network in adult cardiomyocytes*

In cardiomyocytes, the arrangement of mitochondria is remarkably regular, almost like in a crystal, as shown in Fig. 1 (Vendelin et al. 2005; Collins et al. 2002; Aon et al. 2003; Birkedal et al. 2006). This fixed mitochondrial arrangement can easily be shown using a slow speed recording of confocal images. To see whether mitochondria undergo any dynamic changes around these fixed positions, it is necessary to increase the speed of scanning. In our study, the speed of scanning was increased to achieve the pixel dwell time close to 3 μs and intervals between images of 400 ms (see Table 1). At this scanning speed, rapid low

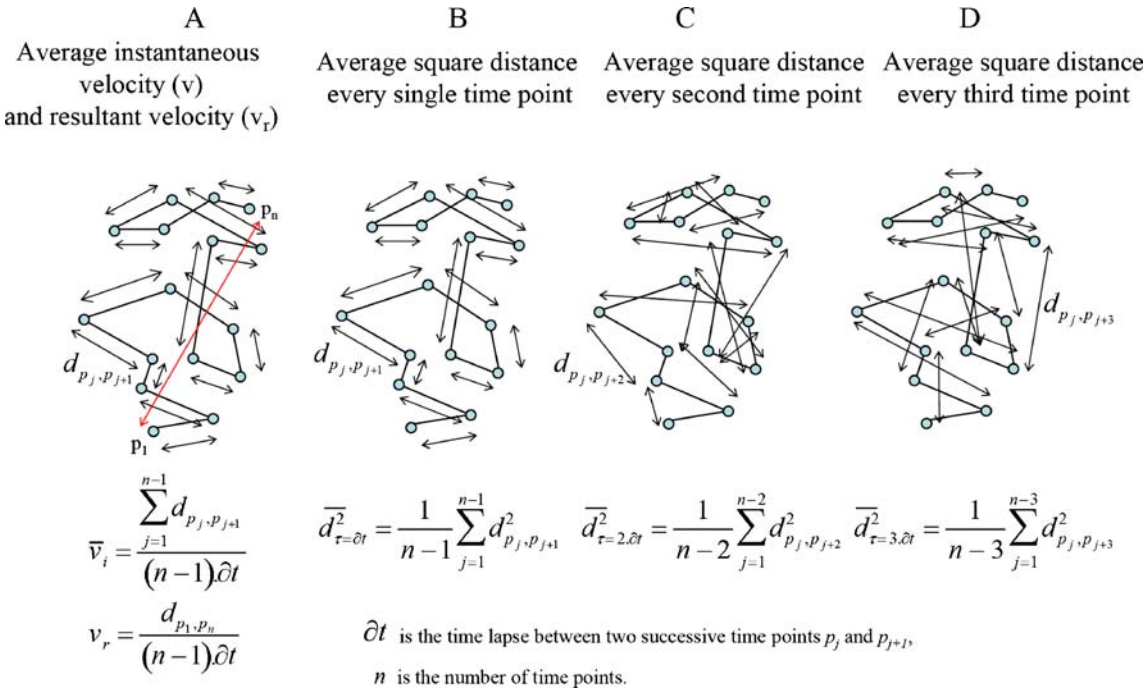


**Scheme 1** Principle of analysis of the velocities of mitochondrial movements in the cells *in situ*. **a** The instantaneous average speed of displacement $v_i$ can be calculated using the distance map method, whereas using Image Correlation Spectroscopy the global speed of displacement-resultant velocity $v_r$ can be calculated (*in red*). These two methods were applied to analyze mitochondrial movement in HL-1 cells. **b**, **c** and **d** Analysis of the random walk (Brownian) movement at three consecutive time points of observations. This method was used for analysis of mitochondrial fluctuations in adult cardiomyocytes

amplitude fluctuations of fluorescence centers in mitochondria was monitored (see Supplementary Material I) using fluorescent molecules (MitoTracker® Green) bound to mitochondrial membranes. As the result of the nature of the calculation procedure to find the fluorescence centers (see "Materials and Methods" section), the positions of these centers depend both on the precise localization of mitochondria in the cells and on the configuration of their inner membrane. The trajectories of the fluorescent centers were plotted to allow visualization of the membrane dynamics (Fig. 2a) and the average scatter parallel to the long (Fig. 2b) and short (Fig. 2c) axis of myocardial cells were calculated for each mitochondrion. The fluorescence intensity inside mitochondria was not homogenous and the position of fluorescence centers' intensity changed in a rather random manner, similar to a random walk movement (Fig. 2a). Interestingly, some clustering of the positions in two distinct areas was observed (Fig. 2a). It was specifically verified that the results obtained in these experiments were not artifacts of recordings like effects of Poisson noise or scanning irregularities. For that the same images series were recorded with the same parameters using green fluorescent beads as references. The results show that the fluctuations of fluorescent centers inside mitochondria are of higher amplitude than the noise recorded with the beads (not shown). Some mitochondria had higher movement amplitudes than others (Figs. 2b and c), corresponding to fluorescence reorganization inside mitochondria, and usually the amplitude of such changes did not exceed 0.2 μm corresponding to ~20 % of a mitochondrion diameter. Very often, the observed changes were even of much smaller amplitude. The changes of axial (x) and transversal coordinates (y) of fluorescence centers of different mitochondria revealed that the amplitude of the axial motion (Fig. 2b) was higher than of the transversal one (Fig. 2c) reaching, in some cases, 0.6 μm. Thus, the motion amplitudes were always inferior to the size of mitochondria which is around 1 μm (see Fig. 1).

Figure 3 shows that in adult cardiomyocytes, where mitochondria have a compact shape and a regular and fixed intracellular arrangement, in strong association with sarcomeres, the movement of fluorescence centers are limited within the range of a mitochondrion's diameter. Figure 3a shows the distribution of all fluorescence centers for all mitochondria in one cell over a 100 s (1 frame/400 ms) observation period,thus summarizing the mitochondrial morphodynamic reorganization (see Supplementary Material II). In Fig. 3a the distribution of fluorescence centers is superimposed with images obtained by conventional low speed scanning microscopy (Fig. 1) which shows whole images of mitochondria and their regular arrangement in cells. In some mitochondria (as the one in the pink frame), the movements are very limited whereas in others (as the one in the blue frame) the movements are much wider (with

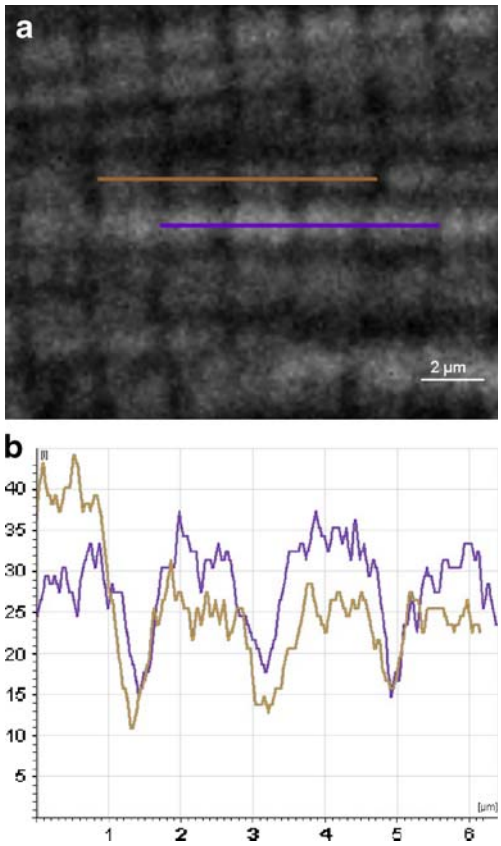


**Fig. 1** Fixed and regular arrangement of mitochondria in adult cardiomyocytes. **a** Confocal image of mitochondrial arrangement in adult cardiomyocytes recorded by low speed scanning after incubation with MitoTracker® Green (*in grey*) during 1 h in Mitomed solution (see "Materials and Methods"). **b** Linear scan of fluorescence intensity profiles of MitoTracker® Green along the lines drawn on image A showing regular mitochondria arrangement in adult cardiomyocytes

higher amplitude), but nevertheless not bigger than the size of a mitochondrion. This suggests that the fluctuations observed are mostly due to changes in the inner membrane configuration. In general, the fluorescence centers do not move from one mitochondrion to another. Thus, Fig. 3a clearly shows that mitochondria in adult cardiomyocytes represent distinct and compact entities, staying very regularly arranged. Their fluorescence centers undergo frequent movements (fluctuations) of very low amplitude restricted to the internal space of mitochondria. These results are in agreement with the absence of mitochondrial fission and fusion events in adult cardiomyocytes.

Similar experiments were repeated with cardiomyocytes permeabilized with saponin and studied in $Ca^{2+}$ -free Mitomed medium (see "Materials and Methods") containing 0.5 mM EGTA and respiratory substrates glutamate and malate but not ADP or ATP. In this medium, the mitochondrial fluorescence center movement was always of random walk type but with somehow smaller amplitudes than in intact non-permeabilized cells (shown in pink frame in Fig. 3a). These results exclude the interpretation of the fluctuations observed due to local changes in $Ca^{2+}$ concentration near mitochondria leading to sarcomere contraction due to spontaneous local $Ca^{2+}$ release from sarcoplasmic reticulum, which, however, may influence the amplitude of the axial movement (blue frames in Fig. 3a).

### *Quantitative analysis of mitochondrial fluctuations in adult cardiomyocytes*

To quantitatively estimate the observed changes in the position of fluoresence centers, stacks of images were recorded from cells during different time intervals at one z plane to visualize 2D movements. The data were then analyzed using the gradient clustering algorithm method. An approximation of random-walk movement based on the Einstein-Smoluchowski theory of diffusion (Philbert 2006; Islam 2004; Agutter et al. 1995; 2000) was applied. This analysis of position changes in mitochondrial fluorescence centers *in situ* was undertaken because these were clearly of random character (see Fig. 2). This allowed the determination of quantitative parameters of these changes, such as the apparent mobility constant D and the movement velocities (see "Materials and Methods" section). For that, the average squared distances ($d^2$) of displacement as a function of lag time (t) were plotted to determine the motion behavior in terms of a random walk process both for low amplitude fluctuations (Fig. 3b) and axial movement (Fig. 3c). The procedure of calculation of displacement distances is described in Scheme 1. Two fitting models were used depending on whether the fluorescent centers' movements have a random walk behavior only for the very low amplitude fluctuations (Fig. 3d, linear model, for mitochondria in pink frame in Fig. 3a and in Fig. 3b, and for mitochondria in permeabilized cardiomyocytes), or a random walk behavior combined with some orientated motion of fluorescent centers over larger distances within mitochondria when recorded for longer time periods (Fig. 3e, polynomial model of second degree, see mitochondria in blue frame in Fig. 3a and their amplitudes in Fig. 3c). Figure 3d shows comparatively the analysis of low amplitude movement for intact and permeabilized cardiomyocytes. In the latter case, the fluctuations were of lower amplitude but with higher rate, showing the influence of metabolites present in cytoplasm in intact cardiomyocytes, probably released during permeabilization. The second degree polynomial model can also be used to fit the trajectories of the fluorescent centers (Fig. 3e) but the second degree term can be eliminated (Fig. 3b) when no higher movement amplitudes of these centers can be observed.

The calculation of apparent parameters of these random-walk processes gave values for the apparent mobility constant D in the range of $1\times10^{-7}\,\mu m^2/s$ to $4\times10^{-6}\,\mu m^2/s$ and the apparent velocity V in the range of $8.5\times10^{-5}\,\mu m/s$ to $2.4\times10^{-4}\,\mu m/s$. For mitochondrial fluctuations in permeabilized cardiomyocytes, the apparent mobility constant was found to

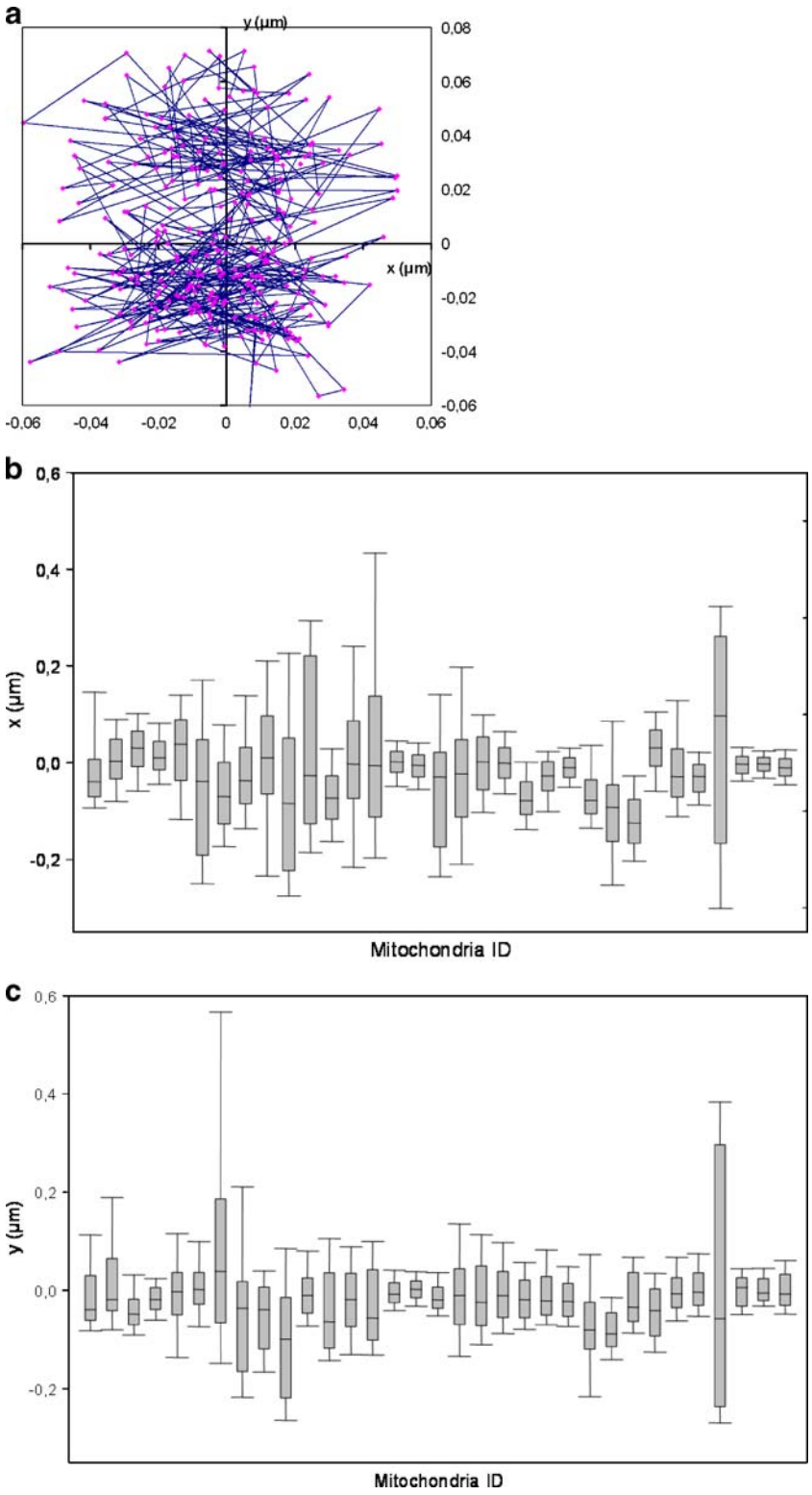


**Fig. 2** **a** Plot of the trajectories of the fluorescence centers of one mitochondrion as a function of recording time. In these confocal experiments, a motion associated with fluorescent molecules (MitoTracker® Green) staining the mitochondria membrane is recorded. The light emitted by a mitochondrion is not homogenous and the position of center fluorescence intensity (mass center) changes randomly. The trajectories of the fluorescent centers were plotted to allow quantitative analysis of membrane dynamics. Each straight line connects the positions of the fluorescence center of a mitochondrion at two consecutive time points (see Scheme 1 and explanations in the text). **b** and **c** Box and whisker plots of coordinates x (**b**) and y (**c**) of the mass centers of 33 different mitochondria inside one cardiomyocyte. The changes of axial (x) and transversal (y) coordinates of mass centers from different mitochondria show that the extent of axial motion (**b**) is bigger than the transversal one (**c**). Notwithstanding, the motion amplitudes are always smaller than the size of a mitochondrion

be increased to $2.5\times10^{-5}\,\mu m^2/s$ to $8\times10^{-4}\,\mu m^2/s$. These results show that the composition of intracellular medium has a clear effect on the quantitative parameters of mitochondrial dynamics and random walk movement of the fluorescence centers.

It has already been shown before by several authors (Aon et al. 2004; Vendelin et al. 2005; Collins et al. 2002; Aon et al. 2003; Saks et al. 2006; Zorov et al. 2000, 2004) that, in adult cardiomyocytes, mitochondria behave as distinct entities and do not form reticular networks. Our results are fully consistent

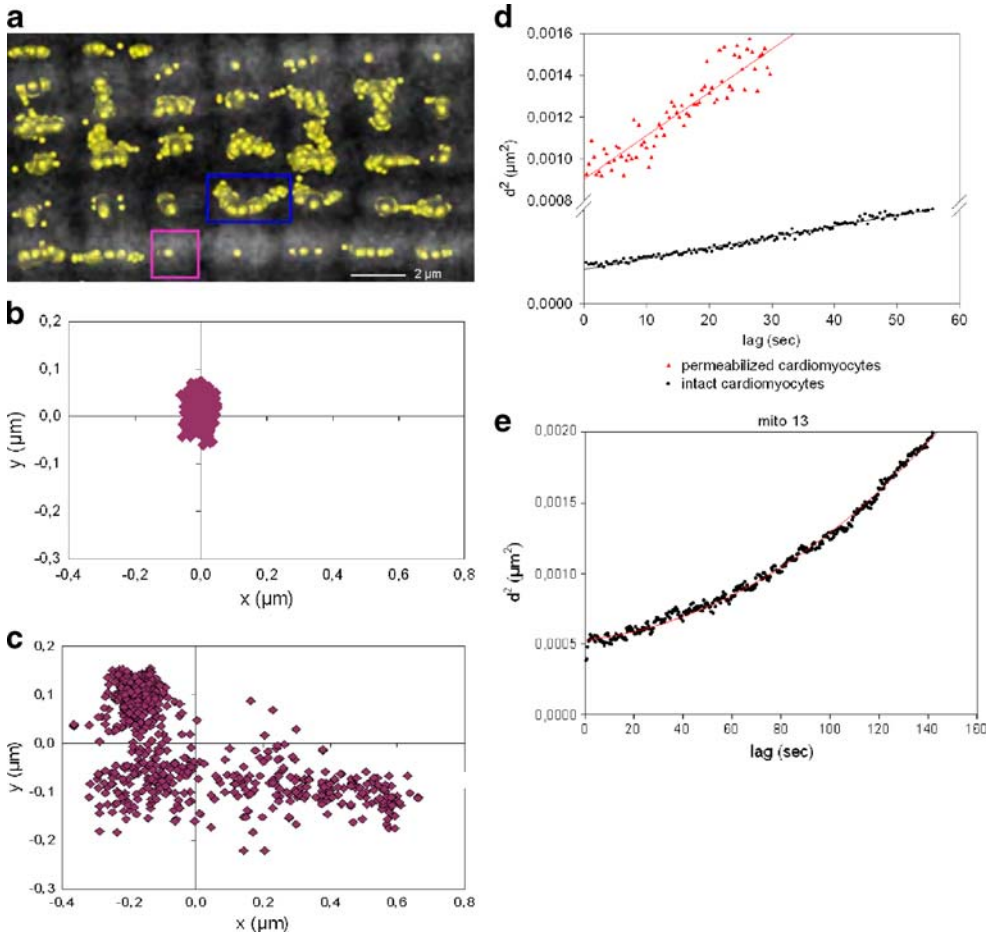


**Fig. 3** **a** Visualization of the positions of mitochondrial fluorescent (mass) centers in a cardiomyocyte over a long time (total duration 100 s) of rapid scanning: movements of fluorescence centers are limited within internal space of mitochondria. Positions of the c fluorescence centers were stacked as a function of time. These fluorescence centers (which are assimilated to the center of mitochondria in cardiomyocytes) are shown as small yellow spheres. The position of fluorescent centers were superimposed with a reference confocal image of MitoTracker® Green fluorescence (*in grey*) showing mitochondrial localization. Note that the fluorescence centers are observed always within the space inside the mitochondria, but from mitochondrion to mitochondrion the motion pattern may differ from very low amplitude motions (*pink frame*) to wider motions distributed over significant space but always within the internal space of a mitochondrion (*blue frame*). **b–e** Quantitative analysis of mitochondrial fluctuations. **b** Plot of the fluorescent center of a given mitochondrion (corresponding at the red square in the Fig. 4) as a function of time. The 0, 0 arbitrary coordinates correspond to the barycenter of all the successive locations of mass centers. For this mitochondrion, the center seems to be randomly distributed as a function of time. **c** Plot of the mass center locations of a second mitochondrion (corresponding to the blue square in the Fig. 3a) as a function of time. For this mitochondrion, the mass center locations seem to cluster in different positions. **d** Graph of the average squared distances ($d^2$) as a function of time for mitochondrial movements in intact cardiomyocytes shown in 3B (black curve), and in mitochondria in permeabilized cardiomyocytes (*red curve*). **e** Graph of average squared distances ($d^2$) as a function time for the same mitochondrion as in D. A 2nd order polynomial model was fitted (*red curve*) to the measurements

with these previously published findings. Precise arrangement of mitochondria can be modified by a controlled proteolytic treatment of permeabilized cardiomyocytes, showing the role of the cytoskeleton in the intracellular organization of mitochondria in adult cardiomyocytes (Vendelin et al. 2005). Spectacular dynamics of mitochondrial shape changes in permeabilized cardiomyocytes after addition of 0.2 µM trypsin are shown in the Supplementary Material III as a movie. There are sudden changes in cardiomyocytes induced by trypsin: after a delay, very rapid and strong contraction is followed by volume increase but the regular arrangement of mitochondria is lost due to successive destruction of cytoskeleton components (proteins) responsible for precise arrangement of mitochondria in the cells. Previously, we have reported that this disorganization is coupled to a decrease of $K_m^{app}$ for exogenous ADP (Kuznetsov et al. 1996; Kay et al. 1997) and thus to a decrease in local restrictions to ADP diffusion (Saks et al. 2003, 2008; Vendelin et al. 2004; Vendelin and Birkedal 2008). The results show that structural modifications of mitochondrial

arrangement induce functional alterations in normal cardiac cells. Interestingly, even after trypsin treatment mitochondria are always of granular form and still, to some extent, in fixed position. Only at much higher trypsin concentration distinct mitochondria could be completely released into the medium. In no case was the fusion of granular mitochondria into filamentous forms observed in our study.

With the aim of verification of these findings concerning the absence of mitochondrial fusion in intact cardiomyocytes under normal conditions, we studied the functional/electrical connectivity of mitochondria.

*Disconnectivity of mitochondria in adult cardiomyocytes*

To assess the question of whether mitochondrial fusion takes place in adult cardiomyocytes, we tested the functional/electrical connectivity of mitochondria in isolated adult rat cardiomyocytes. Indeed, fusion should lead to the formation of a mitochondrial reticulum, thus to electrical continuity between mitochondria (Skulachev 1990, 2001; Skulachev et al. 2004; Amchenkova et al. 1988; Twig et al. 2006; Petronilli et al. 2001). In this study, the mitochondrial membrane potential was monitored using very low concentrations of the specific potentiometric fluorescent probe TMRM, a probe of mitochondrial membrane potential. Similarly to TMRE and JC-1, this dye is widely used for the assessment of mitochondrial inner membrane potential in various cells using different fluorescent techniques such as fluorimetry, FACS, and in particular confocal microscopy (Zorov et al. 2000, 2004; Petronilli et al. 2001; Floryk and Houstěk 1999). In our study, mitochondrial imaging by MitoTracker® Green was performed simultaneously with imaging of TMRM (Fig. 4). Therefore, we could distinguish mitochondria with high or low membrane potential by the intensity of TMRM fluorescence signal together with the mitochondrial imaging performed by MitoTracker® Green staining.

For these co-localization studies, cells were preloaded with TMRM (50 nM) and with MitoTracker® Green (0.2 μM). In control test experiments, dissipation of membrane potential was checked after addition of the respiratory inhibitor antimycin A (5 μM) in combination with the uncoupler FCCP (4 μM), which always strongly decreased TMRM fluorescence (data not shown). Under conditions of normally polarized mitochondria, incubation of cells with TMRM results in its efficient accumulation within the organelle and strong fluorescent signal (red fluorescence). However, under stressful conditions (e.g. by photodynamic ROS production during laser irradiation), mitochondria may lose their membrane potential due to permeability transition (opening of permeability transition pore) (Zorov et al. 2000). In this case, as shown in Fig. 4, the collapse of membrane potential of distinct mitochondria is detected as a strong decrease in TMRM fluorescence, revealing green spots of only MitoTracker® Green labeled

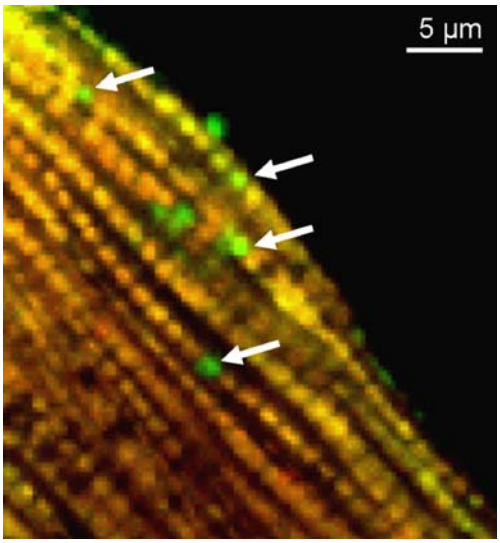


**Fig. 4** Demonstration of the absence of inter-mitochondrial connectivity in cardiomyocytes. Simultaneous image analysis of mitochondria by MitoTracker® Green (*green fluorescence*) and mitochondrial inner membrane potential with TMRM (*red fluorescence*, for details see "Materials and Methods") in adult rat cardiomyocyte. Representative merged image of MitoTracker® Green and TMRM fluorescence shows normally energized and fully depolarized neighboring mitochondria (*indicated by arrows*), which is consistent with the absence of electrical connectivity among them

mitochondria. The latter indicates the existence of mitochondrial neighbours exhibiting different energization status. Notably, these results also confirm that MitoTracker® Green labels all mitochondria independently of their inner membrane potential (Presley et al. 2003). Therefore, the rapid, low amplitude mitochondrial fluctuations observed above can not be related to the oscillations of the membrane potential described in some reports (Cortassa et al. 2004; Hattori et al. 2005). Our results point out that cardiac mitochondria are probably not electrically connected, since distinct individual mitochondria can be depolarized by photo-oxidative stress. This finding confirms that mitochondria within adult cardiomyocytes are electrically unconnected, under normal, non-pathological conditions. These results will also be consistent with differential functional properties among mitochondria within the network (Collins et al. 2002; Collins and Bootman 2003; Kuznetsov et al. 2006) but, at the same time, being metabolically synchronized during excitation/contraction cycles. It has been shown before (Aon et al. 2003, 2006, 2007) that in cardiomyocytes mitochondria form a regular network where they are connected by chemical messengers through diffusion. Under physiological conditions, diffusion of reactive oxygen species (ROS) is likely to be effective in the micrometer range among local neighboring mitochondria.

## Mitochondrial motions in NB HL-1 cells

### *Filamentous organization of the mitochondrial network in NB HL-1 cells*

HL-1 cells were chosen as a reference system for this study because they possess the phenotype of differentiated cardiac cells (Claycomb et al. 1998; Pelloux et al. 2006; White et al. 2006) but they widely differ structurally and metabolically from adult cardiomyocytes. Unlike primary adult cardiac cells, in non-beating (NB) HL-1 cells the creatine effect on respiration was almost absent due to down-regulation of creatine kinase activity. Also, the sensitivity of mitochondrial respiration to exogenous ADP was rather high, close to that of isolated mitochondria, confirming their functional dissimilarity (Anmann et al. 2006; Eimre et al. 2008). This can be related to differences in mitochondrial intracellular organization. Indeed, mitochondria in HL-1 cells are very dynamic, undergoing continual fission and fusion events (Figs. 5 and 6) usually forming long and rapidly moving filamentous structures and highly branched networks (see Fig. 6 and Supplementary Material IV).

### *Analysis of mitochondrial dynamics in NB HL-1 cells*

To quantitatively estimate the rapid mitochondrial movements in NB HL-1 cells, confocal imaging of cells was performed at different time intervals on one *z* plane and analyzed using both image correlation spectroscopy, and the distance map methods.

*Analysis of mitochondrial network dynamics in HL-1 NB cells using the image correlation spectroscopy (ICS) method* If the molecules or particles are mobile, information about mobility can be retrieved by recording a stack of images (assuming that acquisition rate and therefore time resolution is high enough). This approach permits to produce cellular maps of molecular densities, interactions, diffusion rates, and the net direction and magnitude of non-random, concerted molecular movement (Wiseman and Petersen 1999; Wiseman et al. 2005; Margieantu et al. 2000). The local normal or anomalous apparent mobility constants (or velocities) can be determined by fitting temporal autocorrelation functions, averaged over the relevant regions (Fig. 7a). The models of anomalous diffusion and flow appear to be well adapted to characterize the motions of the mitochondrial network in NB HL-1 cells. Indeed, these models are coherent with the mitochondria environment in NB HL-1 cells. The anomalous diffusion model corresponds to a medium with obstacles while the transport (flow) model corresponds to a cytoskeleton-guided mitochondrial movement (Fig. 7b). The validity of the fitting model chosen was confirmed by the high correlation coefficient obtained (= 0.994 with an error RMS=0.00468).

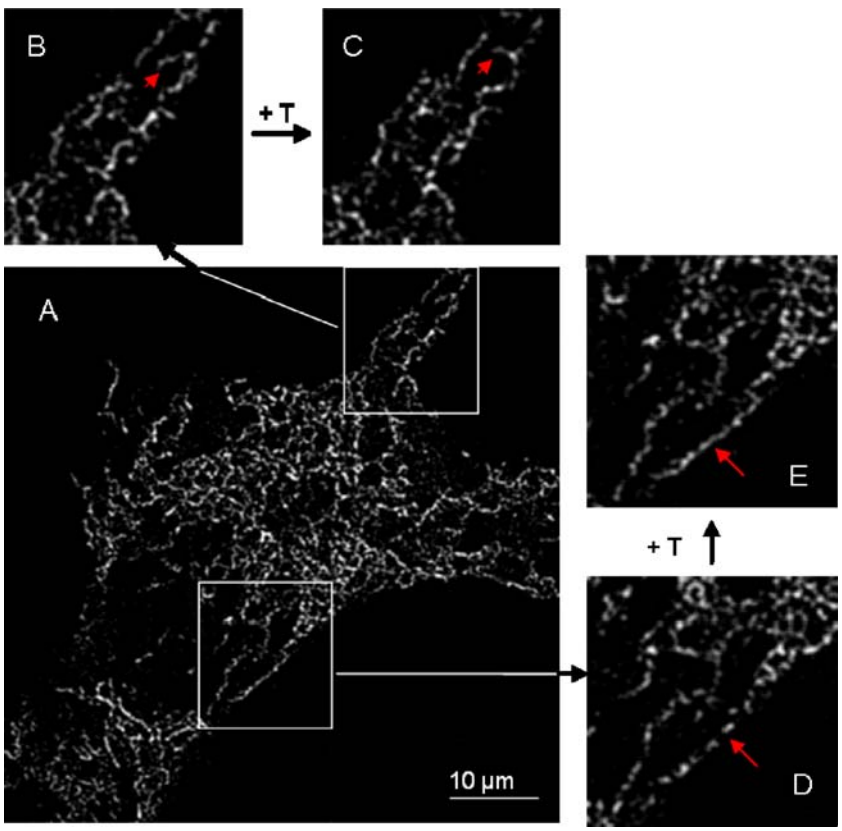


**Fig. 5** Enhanced confocal images of the mitochondrial network in NB HL-1 cells. Mitochondria were stained with MitoTracker® Green (*in white*). In details b, c, d and e, modifications of mitochondria network as a function of time t are depicted. Indeed, mitochondria are very dynamic undergoing continual fission and fusion events usually forming long and rapidly moving filament-like structures

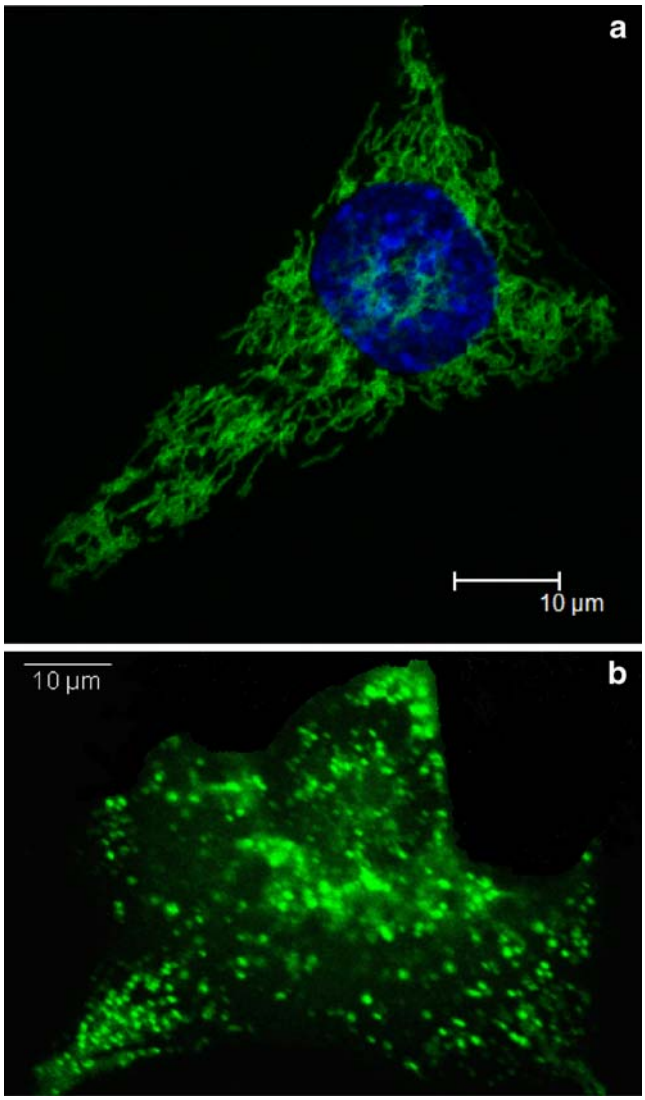


**Fig. 6** **a** Visualization of mitochondrial reticular network with MitoTracker® Green (*in green*) and the nucleus using Hoechst 33342 (*in blue*) in HL-1 cells. **b** Visualization of fragmented mitochondria network in HL-1 NB cells. Confocal images of mitochondria fluorescence stained with MitoTracker® Green

The values of the apparent mobility constant D ($5.6\times10^{-6}$–$7.9\times10^{-5}$ µm$^2$/s) and the apparent flow velocity V ($2\times10^{-4}$ µm/s) were calculated. For NB HL-1 cells, when mitochondria were fragmented (Fig. 6), D was ~$1.2\times10^{-4}$ µm$^2$/s, and $V=6\times10^{-4}$ µm/s. These results show that fragmented mitochondria move faster than non-fragmented mitochondria.

Comparing with the values for adult cardiomyocytes (Fig. 2), the mobility constant is higher in NB HL-1 cells than the one characterizing mitochondrial fluctuations in cardiomyocytes. These results are consistent with the higher degree of freedom of mitochondria in NB HL-1 cells due to the lack of sarcomeres.

*Quantification of mitochondrial movements using the distance map method* The distance map method (Fig. 8) was used to analyze image series of mitochondrial networks to determine the average rates of instantaneous movements of the whole network of a cell or a part of it. Figure 9 shows the results of the average rates of movement of the mitochondrial network (30 experiments). Using this method, the average movement rate value in NB HL-1 cells is 95± 18 nm/s (Fig. 9). Interestingly, these rates are the same order of magnitude as those measured recently in hyppocampal neurons by an optical flow method (Gerencser and Nicholls 2008). These high velocity motions were never seen in adult cardiomyocytes.

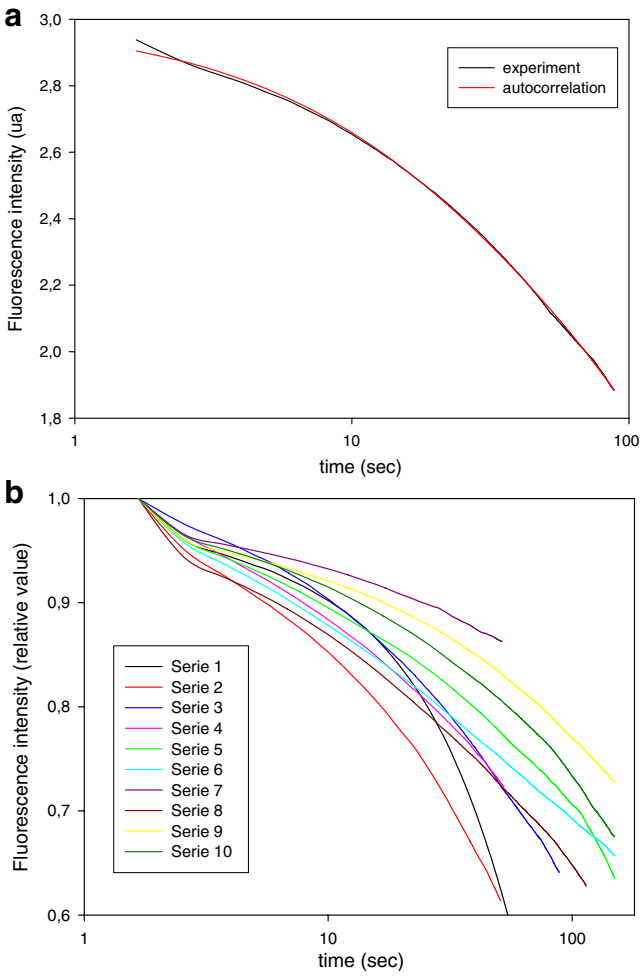


**Fig. 7** **a** ICS analysis of mitochondrial motion in NB-HL-1 cells. This ICS approach and models like anomalous diffusion and flow were used for characterization of the motion behavior of the mitochondrial network in NB HL-1 cells. Experimental autocorrelation curve (*black*) and fitted model (*red*). X-axis: autocorrelation lag time (logarithmic scale), y-axis: fluorescence autocorrelation amount (arbitrary unit). **b** ICS analysis of mitochondrial motion in ten independent series of NB HL-1 cells. The faster the curve plunges (*curves red and black*), the more the resulting global velocity of the cell motion impacts upon the autocorrelation function. x-axis: autocorrelation lag time (logarithmic scale), y-axis : fluorescence autocorrelation amount (arbitrary unit)

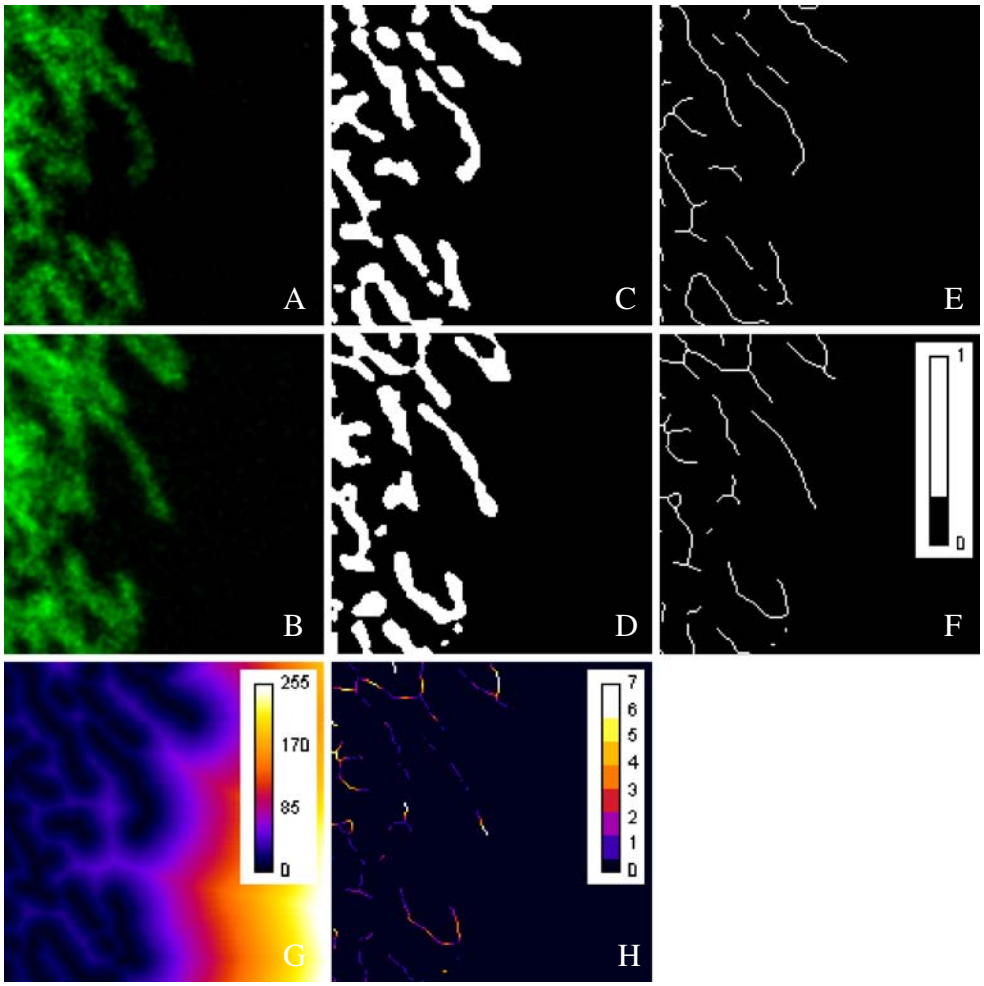


**Fig. 8** Schematic representation of the distance map method for mitochondrial velocity measurement. **a** and **b** Details from confocal images of mitochondria fluorescence at time i and i+1 (image size: 10 µm). **c** and **d** Binary images corresponding respectively to images a and b. **e** and **f** Skeleton images corresponding to images c and d. **g** Map of the distances from the skeleton at time i. **h** Result of the multiplication of images f and g that is projection of skeleton at time i+1 on distance map at time i. The intensity of each pixel in image H corresponds to the distance in pixels ran by mitochondria between times i and i+1

## Discussion

The results of this work show comparatively in adult cardiomyocytes and in NB HL-1 cells the quantitative characteristics of mitochondrial dynamics. In adult cardiomyocytes mitochondria are arranged very regularly in fixed positions by cytoskeletal proteins, as it has been already shown (Vendelin et al. 2005). The novel observation of this work is that, in adult cardiomyocytes under normal conditions, mitochondria, while remaining in rather fixed positions, undergo rapid, low amplitude fluctuations in the positions of their fluorescence centers within the range of less than a mitochondrion's diameter (~20%). The position of fluorescence centers of a dye bound to the mitochondrial inner membrane analyzed in this work depend both on the precise localization of mitochondria in cells, and on the configuration of their inner membrane (see "Materials and Methods" and "Results" sections). Therefore, the rapid, low amplitude, changes in the position of fluorescent centers may reflect frequent and continuous transitions in the configuration of the cristae in the inner mitochondrial membrane.

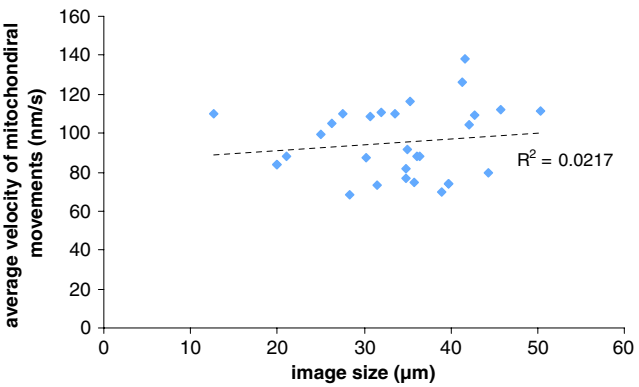


**Fig. 9** Average velocity of mitochondrial movements in NB HL-1 cells using the distance map method. Data obtained from 30 independent experiments and plotted as a function of the the zoom used for image acquisition. Note that the average velocity is independent from the zoom in a wide range (×5 to ×19 with a ×63 objective, corresponding to images of 50–12 µm in width)

Oscillatory phenomena have been very well known in bioenergetics for a long period of time. First observations of heart mitochondrial oscillations were made in Chance's laboratory (Chance and Yoshioka 1966), and oscillations of

fluxes of divalent ions across mitochondrial membranes have been observed in several laboratories (Evtodienko 2000). Loew and collaborators were among the first to apply high resolution quantitative three dimensional microscopy to determine the distribution of potentiometric fluorescent probes between mitochondria and cytoplasm inside living cells (Loew 1993). They observed frequent fluctuations of membrane potential in mitochondria within a 12 mV range around a mean value of 150 mV. Similar spontaneous depolarizations of mitochondria (mitochondrial flickering) were observed by monitoring TMRE responses in smooth muscle cells (O'Reilly et al. 2003). Spontaneous membrane potential fluctuations were also observed in isolated mitochondria (Vergun et al. 2003). By using relative dispersional analysis and power spectral analysis of time series from two photon microscopy of heart cells loaded with TMRM, high-frequency, low-amplitude oscillations in mitochondrial membrane potential were revealed (Aon et al. 2006; Cortassa et al. 2003). The self-sustained and highly coordinated oscillations in membrane potential observed under pathophysiological conditions of oxidative stress (Aon et al. 2003, 2006) could be reproduced in a computational model of ROS-induced ROS release (Cortassa et al. 2003; Aon et al. 2006). Under "physiological" conditions, mitochondrial membrane potential fluctuates at high frequency within a restricted amplitude range, implying depolarization of only microvolts to a few millivolts (Loew 1993; Vergun et al. 2003). Oxidative stress may thus elicit low-frequency, high-amplitude oscillations that characterize the "pathophysiological" response. Very recently, by using the mitochondrial matrix-targeted superoxide indicator, Wang et al. showed the existence of superoxide flashes in individual mitochondria (Wang et al. 2008).

In many of these studies, several fluorescent dyes were visualized by confocal microscopy for mitochondrial localization, the most common of them being TMRM or TMRE. These probes accumulate in mitochondria depending on mitochondrial inner membrane potential when added directly to the cell culture medium. In our studies, to distinguish mitochondrial volume from membrane potential oscillations we used MitoTracker® Green which accumulates in the lipid environment of mitochondria, and is insensitive to membrane potential (see Fig. 4). Rapid random walk-type fluctuations of the fluorescent centers restricted to the size of a mitochondrion likely reflect condensed to orthodox transitions in mitochondrial configuration (Hackenbrock 1966, 1968a, b; Mannella 2001, 2006). A random walk-type mechanism means that the observed fluctuations may be related to probabilities of the independent events within the inner mitochondrial membrane. It was shown in several laboratories (Weber and Blair 1970; Stoner and Sirak 1973; Scherer and Klingenberg 1974) that ligand binding to metabolite carriers in the mitochondrial inner membrane results in structural rearrangements as measured by changes in absorbance. Binding of ADP to adenine nucleotide translocase (ANT) results in contraction of mitochondrial matrix whereas bongkrekate binding provokes matrix expansion. This was explained by changes of carrier localization during ligand binding and metabolite transport across the inner mitochondrial membrane (Weber and Blair 1970; Stoner and Sirak 1973; Scherer and Klingenberg 1974; Klingenberg 2007, 2008). This assumption is illustrated by Scheme 2a which shows a possible connection between changes in position of fluorescence centers as they relate to transitions from condensed to orthodox configuration. Mitochondrial volume fluctuations due to changes from orthodox to condensed configuration during State 4–State 3 transitions correspond to 10–15% volume change for either swelling or contraction, and occur associated with 40–50 mV changes in membrane potential.

Interestingly, in permeabilized cardiomyocytes in Mitomed solution without external ADP and ATP (only intramitochondrial nucleotides were present), the amplitude of fluctuations were smaller but the mobility constant was higher than in intact cardiomyocytes when ATP and ADP were present in cytoplasm (see Fig. 3). The important but rather difficult task for further investigations is to find out how the frequency of fluctuations of mitochondrial fluorescence centers depends upon their functional state (e.g. rate of oxidative phosphorylation, membrane potential, redox state, etc). Further analysis of time series is also needed seeking for long-term correlations not only in the temporal but also in the frequency domain (i.e. after Fourier Transform of the time series) to fully describe the dynamics of mitochondrial volume fluctuations and understand their mechanism.

Scheme 2b illustrates the other principal finding of this study. Only in continuously dividing NB HL-1 cells mitochondria undergo rapid fusion-fission with formation of filamentous reticular structures, characterized by high velocity displacements of mitochondria within the intracellular milieu. In NB HL-1 cells, mitochondria can move very rapidly and theoretically within one minute may displace over a distance exceeding 6 times their diameter (Scheme 2b). In cardiomyocytes, mitochondrial dynamics is limited to changes within intramitochondrial space (Scheme 2b). Thus, in cells with the same cardiac phenotype, mitochondrial fusion and fission can be seen only in cancerous continuously dividing HL-1 cells with altered ultrastructure and energy metabolism (Anmann et al. 2006; Eimre et al. 2008; Pelloux et al. 2006) but not in normal adult cardiomyocytes with crystal-like arrangement of mitochondria, where mitochondrial dynamics is limited to the small-amplitude configuration changes of their inner membrane. Many recent works have shown that mitochondrial fusion and fission are potentially important for cell differentiation and pathophysiology (Yaffe 1999; Dimmer and Scorrano 2006; Kuznetsov 2007; Chan 2006; Chen et al. 2005; Benard and Rossignol 2008;

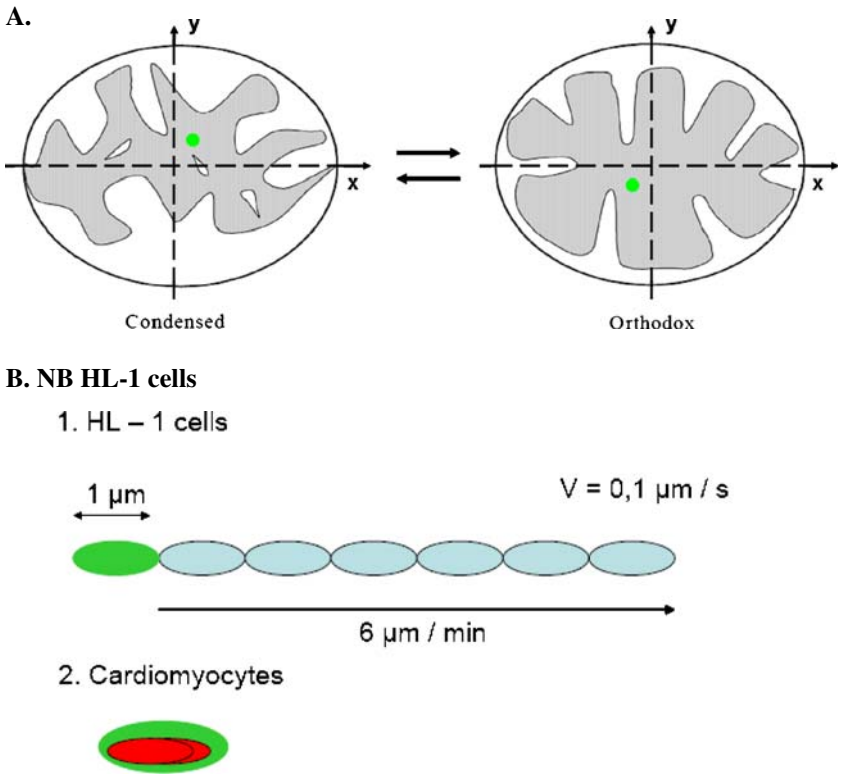


**Scheme 2** **a** Schematic presentation of configurational changes of the mitochondrial inner membrane that may explain the random walk type fluctuations of mitochondrial fluorescence centers. Cristae in the orthodox state (matrix expanded) tend to be tubes or short flat lamellae with one or two junctions in the peripheral region of the inner membrane. Condensed mitochondria (matrix compacted) have larger internal compartments with multiple tubular connections to the peripheral region and to each other. **b** The scheme illustrates the difference in the dynamics and movement of mitochondria in NB HL-1 cells. Mitochondria can move with a velocity enough to displace over a distance exceeding six times their diameter. This is a simplified schematic for the purpose of illustration since the mitochondrial movement in cells may not be linear in just one direction. In adult cardiomyocytes mitochondrial dynamics is limited to the configurational changes of their inner membrane

Karbowski and Youle 2003; Twig et al. 2008a, b). In all these studies, fusion and fission have been carried out mostly in yeast or various cultured cells (easy to grow and use in confocal microscopic studies), when cells are actively dividing. Most mitochondrial imaging studies were performed on tumor-derived cells (e.g. HeLa cells), which may have abnormal bioenergetic properties with possible consequences also for mitochondrial dynamics. Probably for this reason, the general conclusion has been made that fusion and fission phenomena are characteristic and necessary for the normal function of mitochondria (Dimmer and Scorrano 2006; Benard and Rossignol 2008; Twig et al. 2008a, b). This general and rather enthusiastic conclusion is, however, not justified for all cell types. In our study, using fast imaging techniques and specific fluorescent probes, we analyzed the dynamics of mitochondria in cardiomyocytes isolated from adult rat hearts and found no evidence for fusion or fission in non-dividing adult cardiomyocytes during our time scale of observations. It has been directly shown by using matrix-targeted, photoactivatable green fluorescent protein that all areas of a single mitochondrial network are invariably equipotential (Twig et al. 2006). Therefore, if mitochondria would be fused in cardiomyocytes, local depolarization should immediately depolarize all the mitochondrial reticulum, in contradiction with many experimental observations (Aon et al. 2003, 2004, 2006; Collins et al. 2002; Collins and Bootman 2003; Zorov et al. 2000, 2004; Vendelin et al. 2005) (see also Fig. 4).

These results show, in agreement with early work (Aon et al. 2003, 2004, 2006; Collins et al. 2002; Collins and Bootman 2003; Zorov et al. 2000, 2004; Vendelin et al. 2005) that fusion and fission are not necessary for normal functioning of mitochondria of all cell types, and for cardiac cell energetics in particular. This conclusion is in agreement with all experimental evidence obtained during the last 50 years of research in bioenergetics. During these five decades, all laboratories of bioenergetics have successfully isolated mitochondria from heart, liver, skeletal muscle, brain etc. in perfectly granular shape functionally intact and well preserved outer and inner membranes (Hackenbrock 1966, 1968a, b; Mannella 2001, 2006) including Krebs cycle substrates and NADH in the matrix. If mitochondria were in the cells in

fused state (Twig et al. 2008a,b), rapid homogenization of tissue should disrupt all mitochondrial membranes and release Krebs cycle substrates from the matrix. In this case, isolated mitochondria should represent only membrane fragments not able to use Krebs cycle-linked substrates such as pyruvate or glutamate-malate, but capable to directly oxidize NADH. This is never the case if isolation is performed carefully (Hackenbrock 1966, 1968a, b; Mannella 2001, 2006; Rasmussen et al. 2004). Instead, all experimental evidence shows that localization of distinct mitochondria and their regular arrangement in muscle cells are controlled by the cytoskeleton (Milner et al. 2000; Saks et al. 1995, 2007; Appaix et al. 2003; Heggeness et al. 1978; Ball and Singer 1982; Capetenaki 2002; Anesti and Scorrano 2006). In cardiomyocytes, mitochondria form a regular network connected by diffusion of chemical messengers such as ROS between neighboring mitochondria (Aon et al. 2003, 2006, 2007). The contraction process needs a very precise structural organization of sarcomeres and muscle cells (Fukuda et al. 2001; Gordon et al. 2000, 2001; Saks et al. 2006, 2007). Changes in the lattice spacing between acto-myosin filaments in sarcomeres due to alteration of titin orientation are the basis of sarcomere length-dependent activation and the Frank-Straling law (Fukuda et al. 2001; Saks et al. 2006). Mitochondria in muscle cells are in fixed positions determined by their interactions with the cytoskeleton, the sarcoplasmic (Milner et al. 2000) and endo(sarco)plasmic reticulum (Hajnóczky et al. 2000; Pacher et al. 2000; Rizzuto et al. 1998; Appaix et al. 2003; Csordás et al. 2006; Saks et al. 1995, 2007). The cytoskeleton plays an important role for mitochondrial and cell morphology and motility, intracellular traffic, and mitosis (Vale 2003; Vale et al. 1996). Very recently, Rostovtseva et al. (2008) have shown the ability of tubulin to bind directly to the VDAC channel on the outer membrane, controlling the permeability of this channel (Rostovtseva and Bezrukov 2008; Rostovtseva et al. 2008). These interactions are thought to be responsible for mitochondrial regular arrangements into unitary structures (energetic modules, ICEUs) (Saks et al. 2001, 2006, 2007, Seppet et al. 2001; Weiss et al. 2006). These regularly arranged distinct mitochondria localized at the level of A-band of sarcomeres can be easily seen both by electron microscopy (see Fig. 3 in Sommer and Jennings, 1986) and by confocal microscopy (Vendelin et al. 2005; Birkedal et al. 2006). It is not yet completely clear though which components of the cytoskeleton, and to which extent, they are responsible for the regular, modular, arrangement of mitochondria in cardiomyocytes.

Regular arrangement of mitochondria into modular structures (ICEUs) serves an important purpose for survival of heart cells under stressful conditions. Under these circumstances, depolarization and functional damage of separate mitochondria (see Fig. 4) would not result in complete breakdown of cell energetics, since contractile function of the heart will still be maintained by other energetic units which continue to function in a well synchronized manner. The mechanism of this synchronization is still not precisely known and is under active studies in several laboratories (Aon et al. 2007). The differences in the morphodynamics between both mitochondrial network morphologies analyzed in the present work, may not depend only on the type of mitochondria-cytoskeleton interactions but also on signaling properties (e.g. calcium-, ROS-, cAMP-mediated). On the contrary, fusion of mitochondria in heart cells is a clear sign of pathogenesis and cell death. As early as 1969, Sun et al. using electron microscopy showed that hypoxia resulted in the formation of giant mitochondria likely due to fusion in perfused hearts (Sun et al. 1969). This conclusion was recently confirmed by Shen et al. (2007) who showed that mitofusin-2, MFN-2 −is a major determinant of oxidative stress-mediated cardiomyocyte apoptosis (Shen et al. 2007).

In the future, it would be interesting to find out how cytoskeletal proteins, which are responsible for modular organization of mitochondria in adult mammalian cells, interact with proteins responsible for mitochondrial fusion during cardiogenesis, e.g. during formation of adult cardiac cells from stem cells (Chung et al. 2007, 2008).

**Acknowledgements** This work was supported by grant Allocation Doctorale de Recherche PROSPECTIVE N° 05 033206 01 from Région Rhone-Alpes, by grant from Agence Nationale de la Recherche, France, project ANR-07-BLAN-0086-01, by grants from Groupe de Réflexion sur la Recherche Cardiovasculaire, Bristol-Mayers-Squibb, Fondation de France, and by grants N 6142, 7117 and 7823 from Estonian Science Foundation. We would like to thank the Centre Commun de Quantimétrie's team for their precious collaboration and Dr. Dan Sackett, Laboratory of Integrative and Medical Biophysics, Eunice Kennedy Shriver National Institute of Child Health and Human Development, National Institutes of Health, Bethesda, USA, for improving the English.

## Appendix

### Quantitative image analysis of mitochondrial fluctuations within adult cadiomyocytes

Our analysis relies on an iterative gradient clustering algorithm developed for statistics by Fukunaga (Fukunaga and Hostetler 1975) and also referred to in the literature as the mean shift algorithm. Let us consider the image as a collection of pixels $p$ which are defined by a couple of coordinates $x,y$ associated with a fluorescence intensity $w$, also considered as a weight. From this image, we construct a list of points $L$ that will be submitted to the gradient clustering algorithm. In order to reduce the amount of calculations, only those pixels with intensity level greater than a given threshold $t$ are selected.

Let $L$ a set of points $p$, $L = \{p|(x,y)w > t\}$ and $q$ the size of $L$, $(x,y)$ are the coordinates initialized by the pixel location on the image grid.

Let us denote $p_i^k$, the $i^{th}$ point of set $L$ at iteration $k$ ,

Let us consider $G_i^k$ a subset of $L$ containing the points $g^k$ located in the neighborhood of $p^k$: $G_i^k = \left\{g^k \middle| dist\left(p_i^k, g^k\right) < d\right\}$ where *dist* is the Euclidian distance between $p_i^k$, $g^k$; $d$ an arbitrary distance threshold and $n$ the size of set $G_i^k$.

Let us calculate the position $m^k$ of the local center of mass of subset $G$, such that: $m^k = \sum_l^n \left(w_j g_j^k\right) \Big/ \sum_l^n \left(w_j\right)$ with $\Sigma_l^n$ sum from $j=1$ to $j=n$.

Let us denote $\Delta^k$, the local weight gradient vector at point $p_i^k$ such that:

$$\Delta^k = m^k - p_i^k$$

Then we can calculate the new position of point $p^k$ at the next iteration by moving it in direction of the local center of mass $m^k$: $p_i^{k+1} = p_i^k + \alpha\Delta^k \quad 0 < \alpha < 1$, where the shift coefficient $\alpha$ is empirically set for fast convergence and $\Delta^k$ is the local gradient vector at iteration $k$.

Between each iteration step we calculate a total motion criterion as:

$$T^k = \sum_l^q \left\|\alpha\Delta^k\right\|$$

The iteration processed is stopped as soon as $T^k$ becomes smaller than a minimal motion criterion indicating that convergence is reached.

The final step consists in merging the point $p_i$ using a distance criterion, for instance when they cluster within the size of a pixel of the image grid. Then these clustered points are replaced by their center of gravity.

The important parameters to set for this algorithm are the neighborhood criterion, $d$, and the shift coefficient, $\alpha$. There values will impact on the speed and stability of the convergence. Also $d$ must be carefully chosen because the final number of clusters depends on it. Thus a realistic, and object guided choice of $d$ is required. In our case, $d$ was chosen as half of the width of a mitochondrion, making it possible to depict a maximum of two clusters per visible mitochondrion.

## References


Agutter PS, Malone PC, Wheatley DN (1995) Intracellular transport mechanisms: a critique of diffusion theory. J Theor Biol 176:261–272

Agutter PS, Malone PC, Wheatley DN (2000) Diffusion theory in biology: a relic of mechanistic materialism. J Hist Biol 33: 71–111

Amchenkova AA, Bakeeva LE, Chentsov YS, Skulachev VP, Zorov DB (1988) Coupling membranes as energy-transmitting cables. Filamentous mitochondria in fibroblasts and mitochondrial clusters in cardiomyocytes. J Cell Biol 107:481–495

Anesti V, Scorrano L (2006) The relationship between mitochondrial shape and function and the cytoskeleton. Biochim Biophys Acta 1757:692–699

Anmann T, Guzun R, Beraud N, Pelloux S, Kuznetsov AV, Kogerman L, Kaambre T, Sikk P, Paju K, Peet N, Seppet E, Ojeda C, Tourneur Y, Saks V (2006) Different kinetics of the regulation of respiration in permeabilized cardiomyocytes and in HL-1 cardiac cells. Importance of cell structure/organization for respiration regulation. Biochim Biophys Acta 1757:1597–1606

Aon MA, Cortassa S, Marban E, O'Rourke B (2003) Synchronized whole cell oscillations in mitochondrial metabolism triggered by a local release of reactive oxygen species in cardiac myocytes. J Biol Chem 278:44735–44744

Aon MA, Cortassa S, O'Rourke B (2004) Percolation and criticality in a mitochondrial network. Proc Natl Acad Sci USA 101:4447–4452

Aon MA, Cortassa SC, O'Rourke B (2006) The fundamental organization of cardiac mitochondria as a network of coupled oscillators. Biophys J 91:4317–4327

Aon MA, Cortassa S, O'Rourke B (2007) On the network properties of mitochondria. In: Saks V (ed) Molecular system bioenergetics, energy for life. Wiley-VCH, Weinheim, Germany, pp 111–135

Appaix F, Kuznetsov AV, Usson Y, Kay L, Andrienko T, Olivares J, Kaambre T, Sikk P, Margreiter R, Saks V (2003) Possible role of cytoskeleton in intracellular arrangement and regulation of mitochondria. Exp Physiology 88:175–190

Ball EH, Singer SJ (1982) Mitochondria are associated with microtubules and not with intermediate filaments in cultured fibroblasts. Proc Natl Acad Sci USA 79:123–126

Benard G, Rossignol R (2008) Ultrastucture of mitochondria and its bearing on function and bioenergetics. Antioxid Redox Signal 10:1313–1342

Bereiter-Hahn J (1990) Behaviour of mitochondria in the living cell. Int Rev Cytol 122:1–63

Bereiter-Hahn J, Voth M (1994) Dynamics of mitochondria in living cells: shape changes, dislocations, fusion, and fission of mitochondria. Microsc Res Tech 27:198–219

Birkedal R, Shiels HA, Vendelin M (2006) Three-dimensional mitochondrial arrangement in ventricular myocytes: from chaos to order. Am J Physiol Cell Physiol 291:C1148–C1158

Capetenaki Y (2002) Desmin cytoskeleton: a potential regulator of muscle mitochondrial behaviour and function. Trends Cardiovasc Med 12:339–348

Chan DC (2006) Mitochondria: dynamic organelles in disease, aging, and development. Cell 125:1241–1252

Chance B, Yoshioka T (1966) Sustained oscillations of ionic constituents of mitochondria. Arch Biochem Biophys 117:51–465

Chen H, Chomyn A, Chan DC (2005) Disruption of fusion results in mitochondrial heterogeneity and dysfunction. J Biol Chem 280:26185–26192

Chung S, Dzeja PP, Faustino RS, Perez-Terzic C, Behfar A, Terzic A (2007) Mitochondrial oxidative metabolism is required for the cardiac differentiation of stem cells. Nat Clin Pract Cardiovasc Med Suppl 1:S60–7

Chung S, Dzeja PP, Faustino RS, Terzic A (2008) Developmental restructuring of the creatine kinase system integrates mitochondrial energetics with stem cell cardiogenesis. Ann N Y Acad Sci 1147:254–63

Claycomb WC, Lanson NA Jr, Stallworth BS, Eeland DB, Delcarpio JB, Bahinski A, Izzo NJ Jr (1998) HL-1 cells: a cardiac muscle cell line that contracts and retains phenotypic characteristics of the adult cardiomyocyte. Proc Nat Acad Sci USA 95:2979–2984

Collins TJ, Bootman MD (2003) Mitochondria are morphologically heterogeneous within cells. J Exp Biol 206:1993–2000

Collins TJ, Berridge MJ, Lipp P, Bootman MD (2002) Mitochondria are morphologically and functionally heterogeneous within cells. Embo J 21:1616–1627

Cortassa S, Aon MA, Marban E, Winslow RL, O'Rourke B (2003) An integrated model of cardiac mitochondrial energy metabolism and calcium dynamics. Biophys J 84:2734–2755

Cortassa S, Aon MA, Winslow RL, O'Rourke B (2004) A mitochondrial oscillator dependent on reactive oxygen species. Biophys J 87:2060–73

Csordás G, Renken C, Várnai P, Walter L, Weaver D, Buttle KF, Balla T, Mannella CA, Hajnóczky G (2006) Structural and functional features and significance of the physical linkage between ER and mitochondria. J Cell Biol 174:915–921

Dedov VN, Roufogalis BD (1999) Organisation of mitochondria in living sensory neurons. FEBS Lett 456:171–174

Dimmer KS, Scorrano L (2006) (De) constructing mitochondria: what for? Physiology (Bethesda) 21:233–241

Dzeja PP, Chung S, Terzic A (2007) Integration of adenylate kinase and glycolytic and glycogenolytic circuits in cellular energetics. In: Saks V (ed) Molecular system bioenergetics, energy for life. Wiley-VCH, Weinheim, Germany, pp 265–301

Eimre M, Paju K, Pelloux S, Beraud N, Roosimaa M, Kadaja L, Gruno M, Peet N, Orlova E, Remmelkoor R, Piirsoo A, Saks V, Seppet E (2008) Distinct organization of energy metabolism in HL-1 cardiac cell line and cardiomyocytes. Biochim Biophys Acta 1777:514–524

Einstein A (1905) Von der molerulärkinetichen theorie der wärme gefordete bewegung von in ruhenden flüssigkeiten suspendierten teilchen. Ann Phys (Leipzig) 17:549–560

Evtodienko YV (2000) Sustained oscillations of transmembrane $Ca^{2+}$ fluxes in mitochondria and their possible significance. Membr Cell Biol 14:1–17

Floryk D, Houstěk J (1999) Tetramethyl rhodamine methyl ester (TMRM) is suitable for cytofluorometric measurements of mitochondrial membrane potential in cells treated with digitonin. Biosci Rep 19:27–34

Fukuda N, Sasaki D, Ishiwata S, Kurihara S (2001) Length dependence of tension generation in rat skinned cardiac muscle: role of titin in the Frank-Starling mechanism of the heart. Circulation 104:1639–1645

Fukunaga K, Hostetler LD (1975) The estimation of the gradient of a density function, with applications in pattern recognition. IEEE Trans Inf Theory 21(2):32–39

Gerencser AA, Nicholls DG (2008) Measurement of instantaneous vectors of organelle transport: mitochondrial transport and bioenergetics in hippocampal neurons. Biophys J 95:3079–3099

Gordon AM, Homsher E, Regnier M (2000) Regulation of contraction in striated muscle. Physiol Rev 80:853–924

Gordon AM, Regnier M, Homsher E (2001) Skeletal and cardiac muscle contractile activation: tropomyosin "rocks and rolls". News Physiol Sci 16:49–55

Hackenbrock CR (1966) Ultrastructural bases for metabolically linked mechanical activity in mitochondria. I. Reversible ultrastructural changes with change in metabolic steady state in isolated liver mitochondria. J Cell Biol 3:269–297

Hackenbrock CR (1968a) Ultrastructural bases for metabolically linked mechanical activity in mitochondria. II. Electron transport-linked ultrastructural transformations in mitochondria. J Cell Biol 37:345–369

Hackenbrock CR (1968b) Chemical and physical fixation of isolated mitochondria in low-energy and high-energy states. Proc Natl Acad Sci USA 61:598–605

Hajnóczky G, Csordás G, Madesh M, Pacher P (2000) The machinery of local $Ca^{2+}$ signalling between sarco-endoplasmic reticulum and mitochondria. J Physiol 529:69–81

Hattori T, Watanabe K, Uechi Y, Yoshioka H, Ohta Y (2005) Repetitive transient depolarizations of the inner mitochondrial membrane induced by proton pumping. Biophys J 88:2340–9

Heggeness MH, Simon M, Singer SJ (1978) Association of mitochondria with microtubules in cultured cells. Proc Natl Acad Sci USA 75:3863–3866

Islam MA (2004) Einstein-Smoluchowski diffusion equation: a discussion. Physica Scripta 70:120–125

Karbowski M, Youle RJ (2003) Dynamics of mitochondrial morphology in healthy cells and during apoptosis. Cell Death Differ 10:870–80

Kay L, Li Z, Mericskay M, Olivares J, Tranqui L, Fontaine E, Tiivel T, Sikk P, Kaambre T, Samuel JL, Rappaport L, Usson Y, Leverve X, Paulin D, Saks VA (1997) Study of regulation of mitochondrial respiration in vivo. an analysis of influence of ADP diffusion and possible role of cytoskeleton. Biochim Biophys Acta 1322:41–59

Klingenberg M (2007) Transport viewed as a catalytic process. Biochimie 89:1042–1048

Klingenberg M (2008) The ADP and ATP transport in mitochondria and its carrier. Biochim Biophys acta 778:1978–2021

Kuznetsov AV (2007) Structural organization and dynamics of mitochondria in the cells in vivo. In: Saks V (ed) Molecular system bioenergetics, energy for life. Wiley-VCH, Weinheim, Germany, pp 137–162

Kuznetsov AV, Tiivel T, Sikk P, Käämbre T, Kay L, Daneshrad Z, Rossi A, Kadaja L, Peet N, Seppet E, Saks V (1996) Striking difference between slow and fast twitch muscles in the kinetics of regulation of respiration by ADP in the cells in vivo. Eur J Biochem 241:909–915

Kuznetsov AV, Troppmair J, Sucher R, Hermann M, Saks V, Margreiter R (2006) Mitochondrial subpopulations and heterogeneity revealed by confocal imaging: possible physiological role? Biochim Biophys Acta Bioener\getics 1757:686–691

Loew LM (1993) Confocal microscopy of potentiometric fluorescent dyes. Methods Cell Biol 38:194–209

Mannella CA (2001) The relevance of mitochondrial membrane topology to mitochondrial function. Biochim Biophys Acta 1762:140–147

Mannella CA (2006) Structure and dynamics of the mitochondrial inner membrane cristae. Biochim Biophys Acta 1763:542–548

Mannella CA, Buttle K, Marko M (1997) Reconsidering mitochondrial structure: new views of an old organelle. Trends Biochem Sci 22:37–38

Margieantu D, Capaldi RA, Markus AH (2000) Dynamics of the mitochondrial reticulum in live cells using Fourier image correlation spectroscopy and digital video microscopy. Biophys J 79:1833–1849

McBride HM, Neuspiel M, Wasiak S (2006) Mitochondria: more than just a powerhouse. Curr Biol 16:R551–560

Milner DJ, Mavroidis M, Weisleder N, Capetanaki Y (2000) Desmin cytoskeleton linked to muscle mitochondrial distribution and respiratory function. J Cell Biol 150:1283–1298

O'Reilly CM, Fogarty KE, Drummond RM, Tuft RA, Walsh JV Jr (2003) Quantitative analysis of spontaneous mitochondrial depolarizations. Biophys J 85:3350–3357

Pacher P, Csordás P, Schneider T, Hajnóczky G (2000) Quantification of calcium signal transmission from sarco-endoplasmic reticulum to the mitochondria. J Physiol 529:553–564

Pelloux S, Ojeda C, Tourneur Y (2005) An original method to quantify mitochondria movement in cultured cardiomyocytes. Comput Cardiol 32:813–816

Pelloux S, Robillard J, Ferrera R, Bilbaut A, Ojeda C, Saks V, Ovize M, Tourneur Y (2006) Non-beating HL-1 cells for confocal microscopy: application to mitochondrial functions during cardiac preconditioning. Progr Biophys Mol Biol 90:270–298

Petronilli V, Penzo D, Scorrano L, Bernardi P, Di Lisa F (2001) The mitochondrial permeability transition, release of cytochrome c and cell death. Correlation with the duration of pore openings in situ. J Biol Chem 276:12030–4

Philbert J (2006) One and a half century of diffusion: Fick, Einstein, before and beyond. Diffus Fundam 4:6.1–6.19

Presley AD, Fuller KM, Arriaga EA (2003) MitoTracker Green labelling of mitochondrial proteins and their subsequent analysis by capillary electrophoresis with laser-induced fluorescence detection. J Chromatogr 793:141–150

Rasmussen UF, Vielwerth SE, Rasmussen HN (2004) Skeletal muscle bioenergetics: a comparative study of mitochondria isolated from pigeon pectoralis, rat soleus, rat biceps brachii, pig biceps femoris and human quadriceps. Comp Biochem Physiol A Mol Integr Physiol 137:435–46

Rizzuto R, Pinton P, Carrington W, Fay FS, Fogarty KE, Lifshitz LM, Tuft RA, Pozzan T (1998) Close contacts with the endoplasmic reticulum as determinants of mitochondrial $Ca^{2+}$ responses. Science 280:1763–1766

Romashko DN, Marban E, O'Rourke B (1998) Subcellular metabolic transients and mitochondrial redox waves in heart cells. Proc Natl Acad Sci 95:1618–1623

Rostovtseva TK, Bezrukov S (2008) VDAC regulation: role of cytosolic proteins and mitochondrial lipids. J Bioenerg Biomembr 40:163–170

Rostovtseva TK, Hassanzadeh E, Sheldon K, Monge C, Saks V, Bezrukov SM, Sackett S (2008) New role for an old protein: tubulin binding blocks the mitochondrial outer membrane voltage-dependent anion channel and regulates respiration. Proc Natl Acad Sci USA 105:18746–18751

Saks VA, Kuznetsov AV, Khuchua ZA, Vasilyeva EV, Belikova JO, Kesvatera T, Tiivel T (1995) Control of cellular respiration in vivo by mitochondrial outer membrane and by creatine kinase. A new speculative hypothesis: possible involvement of mitochondrial-cytoskeleton interactions. J Mol Cell Cardiol 27:625–645

Saks VA, Kaambre T, Sikk P, Eimre M, Orlova E, Paju K, Piirsoo A, Appaix F, Kay L, Regitz-Zagrosek V, Fleck E, Seppet E (2001) Intracellular energetic units in red muscle cells. Biochem J 356:643–657

Saks V, Kuznetsov A, Andrienko T, Usson Y, Appaix F, Guerrero K, Kaambre T, Sikk P, Lemba M, Vendelin M (2003) Heterogeneity of ADP diffusion and regulation of respiration in cardiac cells. Biophys J 84:3436–3456

Saks V, Dzeja P, Schlattner U, Vendelin M, Terzic A, Wallimann T (2006) Cardiac system bioenergetics: metabolic basis of frank-starling law. J Physiol 571:253–273

Saks V, Monge C, Anmann T, Dzeja P (2007) Integrated and organized cellular energetic systems: theories of cell energetics, compartmentation and metabolic channeling. In: Saks V (ed) Molecular system bioenergetics, energy for life. Wiley-VCH, Weinheim, Germany, pp 59–110

Saks V, Beraud N, Wallimann T (2008) Metabolic compartmentation–a system level property of muscle cells: real problems of diffusion in living cells. Int J. Mol Sci 9:751–767

Scherer B, Klingenberg M (1974) Demonstration of the relationship between adenine nucleotide carrier and the structural changes of mitochondria as induced by adenosine 5'-diphosphate. Biochem 13:161–170

Seppet EK, Kaambre T, Sikk P, Tiivel T, Vija H, Tonkonogi M, Sahlin K, Kay L, Appaix F, Braun U, Eimre M, Saks VA (2001) Functional comlexes of mitochondria with Ca, MgATPases of myofibrils and sarcoplasmic reticulum in muscle cells. Biochim Biophys Acta 1504:379–395

Shen T, Zhen M, Cao C, Chen C, Tang J, Zhang W, Cheng H, Chen KH, Xiao RP (2007) Mitofusin-2 is a major determinant of oxidative stress-mediated heart muscle cell apoptosis. J Biol Chem 282:23354–23361

Skulachev VP (1990) Power transmission along biological membranes. J Membr Biol 114:97–112

Skulachev VP (2001) Mitochondrial filaments and clusters as intracellular powertransmitting cables. Trends in Biochem Sci 26:23–29

Skulachev VP, Bakeeva LE, Chernyak BV, Domnina LV, Minin AA, Pletjushkina OY, Saprunova VB, Skulachev IV, Tsyplenkova VG, Vasiliev JM, Yaguzhinsky LS, Zorov DB (2004) Thread-grain transition of mitochondrial reticulum as a step of mitoptosis and apoptosis. Mol Cell Biochem 256–257:341–58

Sommer JR, Jennings RB (1986) Ultrastructure of cardiac muscle. In: Fozzard HA, Jennings RB, Haber E, Katz AM, Morgan H (eds) The heart and cardiovascular system. Scientific foundations. Raven, New York, pp 61–100

Stoner CD, Sirak HD (1973) Adenine nucleotide induced contraction of the inner mitochondrial membrane. J Cell Biol 56:51–64

Sun CN, Dhalla NS, Olson RE (1969) Formation of gigantic mitochondria in hypoxic isolated perfused rat hearts. Experimentia 25:763–764

Twig G, Graf SA, Wikstrom JD, Mohamed H, Haigh SE, Elorza A, Deutsch M, Zurgil N, Reynolds N, Shirihai OS (2006) Tagging and tracking individual networks within a complex mitochondrial web with photoactivatable GFP. Am J Physiol Cell Physiol 291: C176–C184

Twig G, Hyde B, And Shirihai OS (2008b) Mitochondrial fusion, fission and autophagy as a quality control axis: the bioenergetic view. Biochim Biophys Acta 1777:1092–1097

Twig G, Elorza A, Molina AJ, Mohamed H, Wikstrom JD, Walzer G, Stiles L, Haigh SE, Katz S, Las G, Alroy J, Wu M, Py BF, Yuan J, Deeney JT, Corkey BE, Shirihai OS (2008a) Fission and selective fusion govern mitochondrial segregation and elimination by autophagy. EMBO J 27:433–46

Vale RD (2003) The molecular motor toolbox for intracellular transport. Cell 112:467–480

Vale RD, Funatsu T, Pierce DW, Romberg L, Harada Y, Yanagida T (1996) Direct observation of single kinesin molecules moving along microtubules. Nature 380:451–453

Vendelin M, Birkedal R (2008) Anisotropic diffusion of fluorescently labeled ATP in rat cardiomyocytes determined by raster image correlation spectroscopy. Am J Physiol Cell Physiol 295:C1302–C1315

Vendelin M, Eimre M, Seppet E, Peet N, Andrienko T, Lemba M, Engelbrecht J, Seppet EK, Saks VA (2004) Intracellular diffusion of adenosine phosphates is locally restricted in cardiac muscle. Mol Cell Biochem 256(257):229–241

Vendelin M, Beraud N, Guerrero K, Andrienko T, Kuznetsov AV, Olivares J, Kay L, Saks VA (2005) Mitochondrial regular arrangement in muscle cells: a "crystal-like" pattern. Am J Physiol Cell Physiol 288:C757–767

Vergun O, Votyakova TV, Reynolds IJ (2003) Spontaneous changes in mitochondrial membrane potential in single isolated brain mitochondria. Biophys J 85:3358–3366

von Smoluchowski M (1906) Zür kinetichen theorie der brownschen molekulärbewegung und der suspensionen. Ann Der Physik 21:756–780

Wallimann T, Tokarska-Schlattner M, Neumann D, Epand R, Andres RH, Widmer HR, Hornemann T, Saks V, Agarkova I, Schlattner U (2007) The phosphocreatine circuit: molecular and cellular physiology of creatine kinases, sensitivity to free radicals, and enhancement by creatine supplementation. In: Saks V (ed) Molecular system bioenergetics, energy for life. Wiley-VCH, Weinheim, Germany, pp 195–264

Wang W, Fang H, Groom L, Cheng A, Zhang W, Liu J, Wang X, Li K, Han P, Zheng M, Yin J, Wang W, Mattson MP, Kao JPY, Lakatta EK, Sheu SS, Ouyang K, Chen J, Dirksen RT, Cheng H (2008) Superoxide flashes in single mitochondrion. Cell 134:279–290

Weber NE, Blair PV (1970) Ultrastructural studies of beef heart mitochondria. II. Adenine nucleotide induced modifications of mitochondrial morphology. Biochem Biophys Res Commun 41:821–829

Weiss JN, Yang L, Qu Z (2006) Network perspectives of cardiovascular metabolism. J Lipid Research 47:2355–2366

White SM, Constantin PE, Claycomb WC (2006) Cardiac physiology at the cellular level: use of cultured HL-1 cardiomyocytes for studies of cardiac muscle cell structure and function. Am J Physiol Heart Circ Physiol 286:H823–829

Wiseman PW, Petersen NO (1999) Image correlation spectroscopy. II. Optimisation for ultrasensitive detection of pre-existing platelet-derived growth factor-beta receptor oligomers on intact cells. Biophys J 76:963–977

Wiseman PW, Brown CM, Webb DJ, Hebert B, Johnson NL, Squier JA, Ellisman MH, Horwitz AF (2005) Spatial mapping of integrin interactions and dynamics during cell migration by Image Correlation Microscopy. J Cell Sci 117:5521–5534

Yaffe MP (1999) The machinery of mitochondrial inheritance and behavior. Science 283:1493–1497

Zorov DB, Filburn CR, Klotz LO, Zweier JL, Sollott SJ (2000) Reactive oxygen species (ROS)-induced ROS release: a new phenomenon accompanying induction of the mitochondrial permeability transition in cardiac myocytes. J Exp Med 192: 1001–1014

Zorov DB, Kobrinsky E, Juhaszova M, Sollott SJ (2004) Examining intracellular organelle function using fluorescent probes: from animalcules to quantum dots. Circ Res 95:239–252